prepared for *J. Phys. Chem. C*
revised Jan. 16, 2007

Computational Electrochemistry:

The Aqueous $Ru^{3+}|Ru^{2+}$ Reduction Potential

Pablo Jaque, Aleksandr V. Marenich, Christopher J. Cramer,[1,*] and Donald G. Truhlar[2,*]

Department of Chemistry and Supercomputing Institute, 207 Pleasant St. SE,

University of Minnesota, Minneapolis, MN 55455-0431

Abstract

We present results of density functional calculations for the standard reduction potential of the $Ru^{3+}|Ru^{2+}$ couple in aqueous solution. The metal cations are modeled as $[Ru(H_2O)_n]^{q+}$ surrounded by continuum solvent (q = 2, 3; n = 6, 18). The continuum model includes bulk electrostatic polarization as well as atomic surface tensions accounting for the deviation of the second or third hydration shell from the bulk. After consideration of 37 density functionals with 5 different basis sets it has been found that hybrid and hybrid meta functionals provide the most accurate predictions for the $[Ru(H_2O)_n]^{q+}$ geometries and for the corresponding reduction potential in comparison with available experimental data. The gas-phase ionization potentials of $[Ru(H_2O)_n]^{2+}$ calculated by density functional theory are also compared to results of ab initio computations using second order Møller-Plesset perturbation theory. The difference in solvation free energies of Ru^{3+} and Ru^{2+} varies from −10.56 eV to −10.99 eV for n = 6 and from –6.83 eV to –7.45 eV for n = 18, depending on the density functional and basis set quality. The aqueous standard reduction potential is overestimated when only the first solvation shell is treated explicitly and it is underestimated when the first and second solvation shells are treated explicitly.

[1] email: cramer@chem.umn.edu
[2] email: truhlar@chem.umn.edu

1. Introduction

One of the goals of modern quantum chemical simulations is to understand and predict chemical reactivity, and another is to study the mechanisms of condensed-phase catalytic, electrochemical, and photochemical reactions. Many reactions involve electron transfer steps, sometimes combined with the breaking or formation of chemical bonds. Such reactions are important in environmental chemistry, biochemistry, fuel cells, and electroanalytical field devices. A key thermodynamic variable that describes the tendency of a chemical species to gain or lose electrons is the reduction potential, which may be measured, for example, by cyclic voltammetry or spectrophotometric techniques combined with pulse radiolysis.[1]

Electrochemical phenomena provide a challenge to quantum chemical modeling because the pathway of a reduction-oxidation (redox) reaction can be quite complex, and chemical processes at electrodes (which provide the most quantitative data) can involve several steps such as diffusion and adsorption on the electrode surface. Processes where the most important steps are mass transport of the electroactive species to the electrode surface, electron transfer across the interface, and transport of the product back to the bulk solution allow one to explore the performance of small-molecule computational chemistry methods in estimation of electrochemical parameters like reduction potentials because the rather sophisticated modeling of the electrode-solution interface is avoided. As an example, we consider a redox reaction changing the oxidation state of a transition metal cation in aqueous (aq) solution.

By convention, the reduction potential measures the tendency of a chemical species to acquire electrons and thereby be reduced:

$$O(\mathrm{aq}) + n\mathrm{e}^- \rightarrow R(\mathrm{aq}) \qquad (1)$$

where O and R indicate the oxidized and reduced states of the redox couple $O|R$, respectively. A positive standard reduction potential indicates that the reaction is exergonic ($\Delta G^0_{O|R} < 0$) under the standard conditions (298.15 K, ions at 1 mol/L, gases at partial pressure of 1 atm, and metals in their

pure state). In order to define a consistent electrochemical scale, the standard reduction potential $E^{o}_{O|R}$ is defined as the potential (in volts) at the cathode where the reaction (eq 1) is occurring when the *n* electrons are supplied by oxidation of a reference electrode at the anode in a galvanic cell arrangement. The universal reference electrode is the standard hydrogen electrode (SHE) (also called the normal hydrogen electrode) corresponding to the following reaction

$$H^{+}(aq) + e^{-}(g) \rightarrow \tfrac{1}{2}H_2(g) \tag{2}$$

Then, the standard reduction potential is the potential difference relative to the SHE between the electrodes in a galvanic cell when the redox reaction $O(aq) + n/2\ H_2(g) \rightarrow R(aq) + nH^{+}(aq)$ is measured under standard conditions. In this way, an arbitrary assignment of zero electrode potential is given to the SHE (E^{o}_{SHE} = 0.00 V). $E^{o}_{O|R}$ is related to the standard free energy change relative to the SHE ($\Delta G^{oo} = \Delta G^{o}_{O|R} - \Delta G^{o}_{SHE}$) of the redox process through the following equation:

$$E^{o}_{O|R} = -\frac{\Delta G^{oo}}{nF} = -\frac{\Delta G^{o}_{O|R} - \Delta G^{o}_{SHE}}{nF} \tag{3}$$

where *n* is the number of electrons consumed in the reduction reaction of interest, and *F* is a constant. If free energies are expressed in molar units, then *F* is the Faraday constant (the negative of the charge on one mole of electrons), but if energies are expressed in eV per atom or molecule, as in the present paper, then *F* is equal to the unit charge *e*. $\Delta G^{o}_{O|R}$ is the free energy change associated with eq 1, whereas ΔG^{o}_{SHE} is the free energy change of eq 2; the latter has been established to be −4.28 eV.[2,3]

Recently, we have described computational protocols for use in the theoretical prediction of standard reduction potentials in solution[4–6] based on the thermochemical (Born–Haber) cycle illustrated in Scheme 1. This relates the free energy change in the reduction half-reaction under consideration to the free energy change in the gas phase, ΔG^{o}_{gas} (which equals the adiabatic ionization

potential, I_0^o, of the reduced species plus the 298.15 K thermal contribution, ΔG_{evr}^o, to the free energy of ionization), and standard-state solvation free energies of the oxidized ($\Delta G_S^o(O)$) and reduced ($\Delta G_S^o(R)$) species. Note that I_0^o is the gas-phase enthalpy change for ionization at 0 K. The aqueous standard-state reduction potential referenced to the SHE can then be estimated from the Born-Haber cycle and eq 3 as

$$E_{O|R}^o = \frac{\Delta G_I^o + \Delta\Delta G_S^o + \Delta G_{SHE}^o}{nF} \tag{4}$$

where

$$\Delta G_I^o = I_0^o + \Delta G_{evr}^o \tag{5}$$

where ΔG_{evr}^o is the electronic, vibrational, and rotational contribution to the free energy difference of products from reactants in the top reaction of Scheme 1, and

$$\Delta\Delta G_S^o = \Delta G_S^o(O) - \Delta G_S^o(R) \tag{6}$$

All quantities in eqs 4–6 are at 298.15 K except I_0^o, which is at 0 K. Note that ΔG_S^o has a liquid-phase standard state of 1 mol/L, and we can use a gas-phase standard state of either 1 atm or 1 mol/L, as long as we use the same convention for both *R* and *O*; we will use 1 mol/L. This approach has been successfully applied to organic systems such as quinones, phenols, and anilines; we[4,6] and others[7–29] have shown that continuum solvation models coupled with electronic structure calculations can predict oxidation and reduction potentials for such compounds within about 0.1 V.

In the present study, we develop a computational approach for the prediction of aqueous redox potentials involving metal cations, and the specific system we examine is the $Ru^{3+}|Ru^{2+}$ redox couple. The pioneering study on this kind of problem is the work[30] of Li et al.; they calculated aqueous redox potentials for the $Fe^{3+}|Fe^{2+}$ and $Mn^{3+}|Mn^{2+}$ couples by combining density functional theory (DFT) with continuum dielectric modeling and experimental entropies of di- and trivalent metal cations. They used the BP86[31,32] density functional for discrete cluster models explicitly

involving the first (six water molecules) and second (twelve water molecules) hydration shells along with a continuum solvent model based on the Poisson equation to represent the remaining solvent. They calculated values of $E^{o}_{O|R}$ that in principle converge toward the experimental value when the size of the cluster model is increased. More recently, Uudsemaa et al.[33] have calculated the aqueous redox potential for 3*d* transition metals, again by using the BP86[31,32] exchange-correlation functional for an explicit treatment of the first two hydration shells, but now in conjunction with the COSMO continuum solvent model. Their computational protocol incorporates entropy contributions obtained with the use of $dE^{o}_{O|R}/dT$ from ref 34 as the only empirical electrochemical data in the model, which is capable of reproducing the experimental data with an average absolute error of 0.29 V. The authors[33,35,36] stressed the importance of including the first two solvation spheres explicitly in the metal-water cluster for a better description of the hydration enthalpy of triply charged metal cations. This point has also been emphasized by the authors of other electronic structure based studies of spectral, energetic, and structural properties of hydrated cations.[37–40] However, Uudsemaa and Tamm[33,35,36] found good agreement between one and two hydration shells for doubly charged cations. Holland et al.[41] applied a similar procedure to copper bis(thiosemicarbazonato) complexes.

Another way to calculate reduction potentials is the method recently developed by Sprik and coworkers[42] for treating exchange of electrons between electroactive species and a reservoir (electrode). It is a grand canonical (GC) ensemble modification of the first-principles Car-Parrinello molecular dynamics (CPMD) scheme[43] where the number of electrons is allowed to fluctuate under the constraint of a fixed chemical potential that emulates the reservoir. The method is based on a grand canonical density functional approach that enables one to determine reaction free energies of processes involving exchange of electrons (ionization or attachment) from the response of the molecular system to a variation in the chemical potential of the reservoir; this approach is a direct theoretical model of voltammetric experiments. In this scheme, the elementary process is simulated as an oxidation or reduction half-reaction, where the model system contains the electroactive species

explicitly solvated in either of its two redox states, oxidized or reduced. The redox half-reaction takes place when the electroactive species reaches a crossing between the adiabatic free energy surfaces of the two redox states at some value of the chemical potential. This value of the electronic chemical potential is an estimate of the free energy of the half-reaction under study.

The grand canonical CPMD method has been applied to several redox half-reaction involving transition metal aqueous ions: in particular, $Cu^{2+}|Cu^{+}$ (ref 44); $Ag^{2+}|Ag^{+}$ (refs 44 and 45); $Ru^{3+}|Ru^{2+}$ (refs 46 and 47); $MnO_4^{-}|MnO_4^{2-}$ and $RuO_4^{-}|RuO_4^{2-}$ (ref 48). The accuracy of the results obtained within this method was confirmed by good agreement with experiment for full redox reactions.[44,48] However, an issue that arises about these calculations is whether the realism of the simulations is adversely affected by the way in which the charge is neutralized. In particular, the study of a half-reaction such as eq 1 involves taking one redox active species (*O* or *R*) as a model system in a periodic simulation box filled with solvent molecules, where charge neutrality is maintained by a neutralizing homogeneous background charge density around the cubic MD cell. The small cell dimensions used to keep the molecular dynamics simulations affordable cause the interaction between the ion, its periodic box images, and the compensating background charge to be large, which causes the free energies computed for half-reactions to be dependent on the system size. Such dependence is hidden when full redox reactions, such as $Ag^{2+} + Cu^{+} \rightarrow Ag^{+} + Cu^{2+}$ (ref 44) and $RuO_4^{2-} + MnO_4^{-} \rightarrow RuO_4^{-} + MnO_4^{2-}$ (ref 48) are studied. To some extent, free energies computed for the full redox reactions from the free energies for each of the half reactions calculated separately are in agreement with the experimental data due to partial cancellation of errors.

Here we are interested in studying the following half-reaction:

$$Ru^{3+}(aq) + e^{-} \rightarrow Ru^{2+}(aq) \qquad (7)$$

An experimental value of 0.22 ± 0.03 V was measured by polarography,[49] and the value was re-determined as 0.2487 V by extrapolation of measurements made with a glass electrode.[50] This value is given in two compendia.[50] A later review by Bratsch[34] gives 0.24 V. The most recent

compendium[51] gives 0.23, 0.24, and 0.2487 V. Averaging the four unique values gives 0.23 ± 0.02 V (two standard deviations). This redox reaction is one of those studied by the grand canonical CPMD method of Sprik and coworkers.[46,47] The standard reduction potential calculated by this technique (0.58 V) is overestimated with respect to experiment; however the sign of $E^{o}_{O|R}$ was predicted correctly.[46,47]

In the present work, we estimate the standard reduction potential of the $Ru^{3+}|Ru^{2+}$ couple based on Scheme 1 applied to the following reaction

$$[Ru(H_2O)_n]^{3+}(aq) + e^- \rightarrow [Ru(H_2O)_n]^{2+}(aq) \quad (8)$$

which is the same as eq 7, but with *n* water molecules explicitly included. In particular we consider both $n = 6$, corresponding to an explicit first hydration shell, and $n = 18$, corresponding to treating both the first and second hydration shells explicitly. The nonexplicit water is treated as a dielectric continuum with a nonbulk innermost solvation shell. Note that I^{o}_{0} and ΔG^{o}_{evr} in eq 5 then correspond to the inverse of the following reaction

$$[Ru(H_2O)_n]^{3+}(g) + e^- \rightarrow [Ru(H_2O)_n]^{2+}(g) \quad (9)$$

whereas $\Delta G^{o}_{S}(O)$ and $\Delta G^{o}_{S}(R)$ in eq 6 correspond to

$$[Ru(H_2O)_n]^{q+}(g) \rightarrow [Ru(H_2O)_n]^{q+}(aq),\ q = 2 \text{ or } 3 \quad (10)$$

We have examined the performance of various density functionals classified as follows: generalized gradient approximation (GGA) functionals, hybrid (H) functionals, meta GGA (MGGA) functionals, and hybrid meta (HM) functionals, each combined with various effective core potentials and basis sets for geometry optimizations, vibrational analyses, and electronic structure calculations of aqueous complexes in both oxidation states.

For the continuum solvent model we use the recently developed Solvation Model 6 (SM6),[52] which separates the aqueous solvation free energy into two contributions, one arising from a self-consistent reaction field treatment[53] of long-range bulk electrostatic effects and the other from short-range interactions[54] between the solute and solvent molecules in the first solvation shell. In SM6, the

cavities for the electrostatic calculation and the first solvation shell calculation are defined by superpositions of nuclear-centered spheres whose sizes are fixed (independent of the self-consistent reaction field iterations) and are determined by parameterized radii. Each atom has a separate sphere, unlike the united-atom models used in some other methods. In the present calculation we use a supermolecule (or supersolute) approach (eq 10) in which either the first or the first and second hydration shells are treated as part of the solute; thus, the supersolute already includes one or two explicit solvent shells. Therefore, in the present application, the "first solvation shell" of the SM6 model is actually the second or third solvation shell of the metal cation.

2. Computational Methods

Density Functional Calculations. Geometry optimizations for gas-phase metal-water clusters in both oxidation states were carried out with a variety of density functionals and basis sets. In order to confirm that the resulting geometries correspond to minima on the potential energy surface, vibrational analyses were performed as well. All the DFT calculations were carried out using the *Gaussian03* program (C.01 and D.01 versions).[55]

We tested five basis sets. In all cases the ruthenium cation was described by effective core potentials (ECPs) that replace 28 core electrons with a nonlocal effective potential; the remaining electrons were treated with a basis set of double-ζ or triple-ζ quality. Water molecules were also described with double-ζ and triple-ζ basis sets.

We tested the following basis sets for ruthenium: LANL2DZ,[56] DZQ,[57] TZQ,[58] and MWB28.[59] LANL2DZ incorporates the mass-velocity and Darwin scalar relativistic effects into the ECP, and the basis set for valence electrons is (8*s*6*p*4*d*)/[3*s*3*p*2*d*]. The DZQ and TZQ basis sets use the relativistic ECP of Stevens, Basch, Krauss and Jasien,[57] and the sizes of the valence basis sets are (8*s*8*p*5*d*)/[4*s*4*p*3*d*] and (8*s*8*p*6*d*4*f*)/[4*s*4*p*4*d*3*f*], respectively. MWB28 is a quasi-relativistic

pseudopotential developed by Dolg and coworkers[59] with their corresponding optimized (8*s*7*p*6*d*)/[6*s*5*p*3*d*] valence basis set.

The water molecules in the cluster model were described by the following basis sets: 6-31+G(d,p),[60] MG3S,[61] MG3[62] (MG3S and MG3 are identical to 6-311+G(2df,2p) and 6-311++G(2df,2p) respectively for elements with atomic numbers 14 or lower). The choice of which of these water basis sets was used in the description of the water-metal clusters was made to be consistent with the valence basis set used for ruthenium: (i) LANL2DZ/6-31+G(d,p), (ii) DZQ/6-31+G(d,p), (iii) MWB28/6-31+G(d,p), (iv) TZQ/MG3S, and (v) TZQ/MG3. MWB28/6-31+G(d,p) will be abbreviated MWB28. TZQ/MG3 will be abbreviated, as before,[63] as simply TZQ; TZQ/MG3S will be abbreviated TZQS.

As mentioned in the introduction, the DFT methods we use can be classified into four categories, namely GGA, H, MGGA, and HM. Both GGA and MGGA exchange-correlation functionals depend on the electron spin density and its gradient; MGGA functionals also depend on the spin kinetic energy density. Both H and HM functionals depend on Hartree-Fock exchange, the electron spin density, and its gradient; HM functionals also depend on the spin kinetic energy density. The GGA functionals considered here are: BLYP,[31,64] BP86,[31,32] BPBE,[31,65] BPW91,[31,66] G96LYP,[64,67] HCTH,[68] mPWLYP,[64,69] mPWPBE,[65,69] mPWPW,[66,69] OLYP,[64,70] and PBE.[65] The hybrid functionals that we use are: B3LYP,[31,64,71] B3P86,[31,32] B3PW91,[31,66,72] B97-1,[68] B97-2,[73] B98,[74] BH&HLYP,[31,55,64] mPW1PW,[66,69] O3LYP,[64,70,75] and PBEh.[65,76,77] The meta GGA functionals tested in the present work are: BB95,[31,78] mPWB95,[69] mPWKCIS,[69,79,80] PBEKCIS,[65,79] TPSS (TPSS exchange and TPSS correlation functionals),[81] TPSSKCIS,[79,81] and VSXC.[82] The hybrid meta functionals that we consider here are: B1B95,[31,78] BB1K,[31,78,80] MPW1B95,[69,78,80] MPW1KCIS,[69,79,80] MPWKCIS1K,[69,79] PBE1KCIS,[65,79,83] MPWB1K,[69,78,80] TPSS1KCIS,[66,79–81] and TPSSh.[84,85] Note that mPWPW, mPW1PW, and PBEh are also called mPWPW91, mPW1PW91, and PBE1PBE, respectively; mPW1PW is also called MPW25, and PBEh is also called PBE0.

In the case of Ru^{q+} and $[Ru(H_2O)_n]^{3+}$, which have an unpaired electron, the spin-unrestricted approach is employed for all calculations in the present study. For $[Ru(H_2O)_n]^{2+}$ we used spin-restricted solutions with all orbitals doubly occupied.

We first calculate the gas-phase adiabatic ionization potentials and the 298.15 K thermal contribution to the free energy change for the process of eq 9 (n = 6, 18). The contribution of the cation complexes to ΔG^{o}_{evr} in the gas phase was calculated by standard formulas (using *Gaussian03*[55]), and the contribution of the electron to ΔG^{o}_{evr} at 298.15 K is less than 0.001 eV.[86] The vibrational-rotational contribution to ΔG^{o}_{evr} can be computed in the harmonic-oscillator-rigid-rotor model, but the result is a sensitive function of the frequencies of vibrational modes with frequencies below 100 cm^{-1}. We calculated vibrational frequencies for 370 cases with n = 6 (q = 2 or 3, five basis sets, 37 functionals) and for 294 of the cases with n = 18; we found that the lowest frequency varies from 30 to 131 cm^{-1} for n = 6 and from 26 to 55 cm^{-1} for n = 18. The trends in ΔG^{o}_{evr} due to these and other low-frequency modes are not necessarily meaningful in the absence of a reliable treatment of anharmonicity, which is impractical. The average value of the harmonic ΔG^{o}_{evr} (averaged over the 185 cases for n = 6) is –0.04 eV, with a standard deviation of 0.02 eV. Therefore we simply approximated ΔG^{o}_{evr} as –0.04 eV for all cases with n = 6. The average value of the harmonic ΔG^{o}_{evr} for the 147 cases where we have frequencies for both q = 2 and q = 3 for n = 18 is –0.01 eV with a standard deviation of 0.07 eV, and we simply used –0.01 in all of these cases.

We also investigated different spin multiplicities for the ground state of aqueous complexes and found that the ground states are the low-spin (d^6) singlet for $[Ru(H_2O)_n]^{2+}$ and the low-spin (d^5) doublet for $[Ru(H_2O)_n]^{3+}$ whereas the bare Ru^{2+} and Ru^{3+} cations in their ground states correspond to the terms ^5D and ^6S, respectively. The transformation of the high-spin bare cation to a low-spin complex is a well known effect for inorganic complexes, and is explained by means of ligand

(crystal) field theory.[87] It provides a reminder that solvation of a transition metal cation is not only a result of weak noncovalent interactions but also a chemical reaction.

Aqueous Solvation Free Energies. The aqueous solvation free energies ΔG_S^o for water-metal clusters in both oxidation states were calculated at the SM6/DFT level using gas-phase geometries. The solvation free energies for the gas-phase geometries obtained with TZQS and TZQ were calculated with the MWB28 basis because SM6 was parameterized for the 6-31+G(d,p) basis set but not for MG3 and MG3S.

In the SM6 implicit solvation model, ΔG_S^o is partitioned into two contributions:

$$\Delta G_S^o = \Delta G_{EP} + G_{CDS} + \Delta G_{Conc}^o \quad (11)$$

where the first term accounts for the bulk electrostatic effect, which is long-ranged and is calculated by a self-consistent reaction field procedure; this term contains the change in the internal free energy of the solute upon solvation, the free energy of polarization, and the free energy cost of polarizing the solvent.[88] SM6 uses a new charge model, which is called CM4,[52] to assign partial atomic charges in the electrostatic part of the calculation. The second term in eq 11 accounts for cavitation, dispersion, solvent-structure effects (CDS) beyond those involved in bulk electrostatic polarization, and other effects beyond bulk electrostatics; this term is estimated from the solvent accessible surface area (SASA) of the solute (supersolute) and a set of empirical atomic surface tensions that depend on its geometry. The third terms in eq 11 is zero in the present article because we use the same concentration (Conc) in the gas phase and liquid solution. It would not be zero if we used 1 atm for the gas-phase standard state; it would be +1.89 kcal/mol.

Since the CM4 model does not have parameters for Ru, these parameters were set to zero. This simply means that the partial atomic charge on Ru is given by an unmodified Löwdin population analysis.[89] Furthermore, the SM6 solvation model does not have parameters for Ru. We therefore set the Ru radius to 2.0 Å (see Section 4 for details) and the Ru atomic surface tension to zero. The calculated free energies are very insensitive to both of these quantities because the ruthenium atom

has very little solvent accessible surface area (SASA) in the water complexes. In particular, depending on the density functional and the basis set, the SASA of Ru in $[Ru(H_2O)_6]^{q+}$ is in the range of 2.75 – 3.13 Å^2 for q = 2 and 1.67 – 1.86 Å^2 for q = 3. With n = 18 these values decrease to 0.96 – 1.22 Å^2 for q = 2 and 0.62 – 0.80 Å^2 for q = 3. The effect of varying the ruthenium radius or including the ruthenium atomic surface tension will be examined in Section 4.

Standard SM6 radii of 1.52 and 1.02 Å were used for the oxygen and hydrogen atoms, respectively.

All of the SM6 calculations were carried out with MN–GSM.[90]

Wave Function Theory Calculations. In order to check the validity of DFT predictions, we performed a few single-point energy computations for bare ruthenium cations Ru^{q+} and for the $[Ru(H_2O)_n]^{q+}$ clusters (n = 6, 18; q = 2, 3) using wave function theory (WFT), in particular second-order Møller-Plesset perturbation theory (MP2)[91,92] and coupled cluster theory (CCSD,[93] CCSD(T),[94] and CCSDT[95]). The MP2 calculations were carried out with *Gaussian03*,[55] and the coupled cluster calculations were done with ACESII.[96] We employed spin-restricted formalisms for an even number of electrons and spin-unrestricted orbitals for an odd number of electrons. We also employed the GAMESS program[97] for complete active space self-consistent field (CASSCF) calculations of selected molecular structures of $[Ru(H_2O)_n]^{3+}$ as well as for computation of the spin-orbit splitting in ^{5}D Ru^{2+} and ^{2}D Ru^{3+} by means of perturbative solution of the full Breit-Pauli spin-orbit operator[98] with a CASSCF reference wavefunction. The spin-orbit coupling calculation was carried out with inclusion of one- and two-electron scalar relativistic effects treated by means of elimination of the small components of relativistic wavefunctions (the RESC scheme).[97,98] No frozen core approximation was used for electron correlation beyond an effective core potential replacing the core orbitals $1s^2 2s^2 2p^6 3s^2 3p^6 3d^{10}$ of Ru.

3. Results and Discussion

3.1 Molecular Structure

Conformations of water-metal clusters that include the first and second coordination spheres were optimized in the absence of a continuum solvent. Experimental[99,100] and theoretical[101,102] evidence suggests that the first solvation shell of 4*d* transition metals ions is composed of six water molecules. Information on the second coordination shell is much scarcer than for the first hydration shell; however, many hydrated ions have a second solvation shell of 12 water molecules,[100,103] and we optimized several structures with a second hydration shell of twelve water molecules.

$[Ru(H_2O)_6]^{q+}$ (q = 2, 3). In the present study, we identified three stationary points on the potential energy surfaces of ruthenium clusters with six water molecules. These structures are displayed in Figure 1. The lowest energy structures for $[Ru(H_2O)_6]^{2+}$ have C_i and S_6 symmetry (see Figure 1*a* and 1*b*, respectively). These conformations are geometrically and energetically very close; the energy difference between the two minima is approximately 0.01 eV in favor of the C_i structure at all levels of theory used in this work. Vibrational analysis shows that the T_h configuration similar to the C_i structure is a higher order saddle point for the divalent cluster (d^6).

In the case of $[Ru(H_2O)_6]^{3+}$, we have found only one minimum that corresponds to C_i symmetry. To resolve an issue whether higher symmetry (T_h and S_6) configurations could be stationary points on the potential energy surface of $[Ru(H_2O)_6]^{3+}$ (d^5) we performed the CASSCF/MWB28 energy calculation for the ground and excited electronic states at the T_h and S_6 equilibrium geometries optimized for the divalent complex (d^6) and described above. The complete active space consisted of five electrons in five molecular orbitals approximately corresponding to *d*-orbitals of the ruthenium atom with a spin multiplicity of 2. The T_h structure corresponding to the ground electronic state $\tilde{X}\,^2T_g$ cannot be a stationary point, being subject to Jahn-Teller distortions[104] along the nuclear coordinates of t and e symmetry types breaking the T_h symmetry in the trigonal and tetragonal directions, respectively. In the case of nuclear configurations of $[Ru(H_2O)_6]^{3+}$ with S_6 symmetry, the ground electronic state $\tilde{X}\,^2A_g$ is strongly coupled with the low-lying first excited state $\tilde{A}\,^2E_g$ and cannot be adequately treated by a single-reference approach, at least without special

procedures (we experienced problems with SCF wavefunction symmetry breaking and convergence in the DFT calculations). Further analysis of the T_h and S_6 symmetry configurations of $[Ru(H_2O)_6]^{3+}$ is beyond the scope of the present study because these structures are predicted to lie higher than the global minimum for the trivalent complex corresponding to lower symmetry (C_i). The ground electronic state $\tilde{X}\,^2A_g$ at the C_i symmetry nuclear configuration is well-isolated from the first excited state $\tilde{A}\,^2A_g$ with a vertical excitation energy of 0.3 eV (CASSCF/MWB28).

Table 1 shows average equilibrium Ru–O bond distances optimized with a variety of density functionals and basis sets for the $[Ru(H_2O)_6]^{q+}$ clusters in both oxidation states. Comparison of these distances to the experimental values measured[105] for dilute solution by the extended X-ray absorption fine structure method (2.11 Å for Ru^{2+} and 2.03 Å for Ru^{3+}) indicates that all 185 calculations overestimate the metal-ligand distances for both charge states. Marcos et al.[106] studied the effect of the solvent reaction field on the geometry of several aqua metal cations and observed that the solvent reaction field decreased the M–O bond distances by 0.020 – 0.050 Å, which is in the correct direction to correct this systematic error. Table 1 also gives the average mean unsigned error (AMUE) for density functionals, averaged over basis set and charge state, and the average unsigned error (AUE) for each basis set with each category of functionals. Averaged over basis sets, the AMUEs calculated for the various functionals range from 0.026 to 0.082 Å. The HM functionals are the most accurate ones in comparison with available experimental data[105] for the Ru–O bond distances in both oxidation states, whereas the H functionals are the next most accurate ones on average. According to the errors for each of the basis sets used in this study, the MWB28 basis set generally gives the best theoretical predictions of Ru–O in respect to experiment,[105] followed in order by TZQ, TZQS, LANL2DZ, and DZQ. The combination of MWB28 (for Ru) and 6-31+G(d,p) (for H and O) also has a lower computational cost than the TZQ/MG3S or TZQ/MG3 basis sets.

The best performing density functional for geometries of the aqua ruthenium complexes in both oxidation states is MPWB1K (a type HM functional) with errors of 0.020 Å for the MWB28,

TZQS, and TZQ basis sets; these results are more accurate than those obtained in the grand canonical CPMD study reported by Sprik et al.[46,47] where the mean unsigned error is 0.07 Å. The VSXC (a type MGGA functional) and BLYP (of type GGA) functionals are the least accurate methods of the 37 studied density functionals for Ru–O distances for di- and trivalent ruthenium-water complexes. This finding is especially relevant because Sprik et al., in their grand canonical CPMD simulations,[46,47] used the BLYP functional in combination with a plane wave basis set and a pseudo-potential constructed according to the Troullier-Martins scheme.[107] Our Ru–O bond distances obtained here with the BLYP functional combined with five basis sets agree with their bond distances (see in refs 46 and 47: 2.18 Å for Ru^{2+} and 2.10 Å for Ru^{3+}) on average within 0.4%, and our values obtained with the three larger basis sets (MWB28, TZQS, and TZQ) agree with theirs on average within 0.3%, when we use the BLYP functional.

$[Ru(H_2O)_{18}]^{q+}$ (q = 2, 3). Experimental information on the structural details of the second hydration shell is scarcer in comparison with that for the first shell. However, X-ray diffraction measurements of some di- and trivalent salts suggest that the size of the second hydration shell is around 12 water molecules.[100,103] When the second coordination sphere is included in the cluster, we consider several models of hydrated ruthenium ions with six water molecules in the inner shell and 12 molecules in the outer coordination sphere as displayed in Figure 2. Figure 2*a* illustrates a sandwich-like structure with a dense network of hydrogen bonds, where each water molecule of the inner shell is bonded to two ligands in the second coordination sphere. This structure has S_6 symmetry and it has already been reported for other hydrated transition metals,[33,35] aluminum,[40,108] and alkaline-earth ions.[39,108] Figure 2*b* displays a conformer of C_3 symmetry; it is characterized by two water trimers and three water dimers in the outer hydration shell; the last fragments are oriented quasi-linearly with the metal ion. This structure has a less dense network of hydrogen bonds than the former one. Another structure of C_3 symmetry is that shown in Figure 2*c*, where the outer solvation sphere can be broken down into five groups of water molecules. Two of them are formed by three molecules and each of the others are composed of two molecules; this conformer is more compact than the C_3 one

previously described. Finally, we also explored the T_h symmetry structure used by Li et al. in their study[30] of hydrated iron and manganese ions, which is indicated by Figure 2*d*.

The three molecular structures of S_6 and C_3 symmetry optimized for the divalent complex $[Ru(H_2O)_{18}]^{2+}$ (d^6) with two explicit solvation shells at the BLYP level of theory are found to be minima on the potential energy surface whereas the T_h symmetry complex corresponds to a higher order saddle point according to the harmonic analysis of these stationary points. The structure of S_6 symmetry is more stable than either of the C_3 symmetry conformers shown in Figure 2*b* and 2*c* by 0.35 eV and 0.48 eV, respectively (BLYP/MWB28).

Only the S_6 structure was located as a minimum on the potential energy surface for the trivalent complex (d^5). The optimizations for other conformers were also carried out without symmetry constraints to allow a full reorganization of the two coordination spheres, but we did not find additional low-lying stationary points. According to a CASSCF calculation of the $[Ru(H_2O)_{18}]^{3+}$ electronic structure, the first excited electronic state $\tilde{A}\ ^2E_g$ is well-separated (~0.5 eV) from the ground state $\tilde{X}\ ^2A_g$. Unlike the case of $[Ru(H_2O)_6]^{3+}$, a coupling of the ground and excited electronic states of $[Ru(H_2O)_{18}]^{3+}$ has no noticeable impact on the SCF convergence at least in the vicinity of the minimum corresponding to the S_6 structure so that a one-reference approach (for instance, DFT) can safely be applied to the study of the open-shell $[Ru(H_2O)_{18}]^{3+}$ complex. As in the case of $\tilde{X}\ ^2T_g$ $[Ru(H_2O)_6]^{3+}$, the T_h symmetry structure of $[Ru(H_2O)_{18}]^{3+}$ undergoes Jahn-Teller distortion[104] and cannot be a stationary point of any kind.

As shown above, according to the BLYP calculations of various structures depicted in Figure 2, the $[Ru(H_2O)_{18}]^{q+}$ cluster including the first and second hydration shells has a global minimum of S_6 symmetry in both oxidation states. The S_6 symmetry configurations were optimized using DFT methods and basis sets of varying quality. Table 2 shows Ru–O bond distances corresponding to the first coordination shell in the $[Ru(H_2O)_{18}]^{q+}$ cluster. As in the case of $[Ru(H_2O)_6]^{q+}$, the MPWB1K functional provides the most accurate theoretical prediction of the $[Ru(H_2O)_{18}]^{q+}$ geometries in

comparison with available experimental data (see in ref 105: 2.11 Å for Ru^{2+} and 2.03 Å for Ru^{3+}). The results in Table 2 show the influence of the second coordination sphere on the Ru–O distance in the first coordination shell: inclusion of the second shell leads to slightly shorter Ru–O distances within the $[Ru(H_2O)_6]^{3+}$ core, whereas a weaker effect is observed for the corresponding distances in the divalent complex with 18 water molecules. As a consequence of this effect, the present BLYP results are again in close agreement with results of the BLYP study[46,47] of Sprik et al. including 32 water molecules (see in refs 46 and 47: 2.18 Å for Ru^{2+} and 2.10 Å for Ru^{3+}). In particular, the Ru–O distances calculated in the present study agree on average within 0.3% with the results of the previous calculations.[46,47] Again, the functional used in refs 46 and 47 is found to be less accurate than many others used in our study. One of the disadvantages of the CPMD methods is that *hybrid* and *hybrid meta* functionals, which are often more accurate, tend to be avoided as being either impractical or too expensive.

3.2 Gas-Phase Free Energies

The Ru^{2+}, Ru^{3+} Cations. First we examined the performance of different density functionals and effective core potentials for the calculation of the third ionization potential of the bare ruthenium atom. The high-spin states ^{5}D Ru^{2+} and ^{6}S Ru^{3+} were found to be more stable than the corresponding low-spin states ^{1}S Ru^{2+} and ^{2}D Ru^{3+} by 3.33 and 5.37 eV, respectively, at the CCSD(T)/TZQ level.

Table 3 lists computed values of the third ionization potential of Ru for a selection of density functionals and compares them to experiment.[109] The DFT numbers were corrected by adding the value of 0.13 eV (1073 cm^{-1}) corresponding to the spin-orbit splitting in ^{5}D Ru^{2+} calculated with the full Breit-Pauli spin-orbit operator and accounting for scalar relativistic effects (see Section 2 for details) using all-electron DZVP basis set[110] that was totally uncontracted [18*s*,12*p*,9*d*] (uDZVP). This predicted spin-orbit splitting (1073 cm^{-1}) is very close to the value of 1061 cm^{-1} in ^{5}D Ru^{2+} derived from the electronic spectrum of Ru^{2+} as given in the compilation of Moore.[109] Unlike ^{5}D Ru^{2+}, the spin-orbit splitting calculated in the low-spin state ^{2}D Ru^{3+} is very small (17 cm^{-1}).

In comparing theory and experiment with respect to the third ionization potential for the bare ruthenium atom, one should note that the corresponding reference values[109] can have some uncertainty beyond the standard error of measurements because they were not directly measured but extrapolated by a Ritz formula (28.01 eV) or by comparison of the spectra of ionic species from Y^{2+} to In^{2+} (28.47 eV).[109] Almost all the exchange-correlation functionals significantly overestimate the third ionization potential with any of the basis sets (up to 1.27 eV at the B3P86/LANL2DZ level), whereas BH&HLYP, VSXC, MPWKCIS1K, and TPSSh (mostly, with DZQ and MWB28 basis sets) provide better agreement with the reference data.[109] LANL2DZ calculations are the least accurate of those considered in this work (Table 3). Values of the third ionization potential of Ru calculated using DFT methods are also overestimated (by 0.5 – 2.0 eV) in comparison with the values of 27.81 eV and 27.79 eV calculated using CCSDT/TZQ and MP2/TZQ, respectively.

The role of scalar relativistic effects in these calculations was investigated by means of computation of the Darwin and mass-velocity corrections (see ref 96 and references therein) at the CCSD(T)/uDZVP level of theory. The total scalar relativistic correction to the ionization potential value calculated using an all-electron basis set with no relativistic effects included is quite large (−0.41 eV). This indicates the importance of using relativistic effective core potentials that account for the relativistic effects arising from contraction of the inner electronic shells of the ruthenium ions.

$[Ru(H_2O)_n]^{q+}$ (n = 6, 18; q = 2, 3). Tables 4 and 5 list the free energies $\Delta G_{\mathrm{I}}^{\mathrm{o}}$ of ionization of the gas-phase $[Ru(H_2O)_n]^{2+}$ clusters with explicit treatment of the first hydration shell (n = 6) and the first and second shells (n = 18), respectively. All the values were calculated at 298.15 K, and include the corresponding zero-point energy and thermal corrections $\Delta G_{\mathrm{evr}}^{\mathrm{o}}$. The latter are usually small, as discussed in Section 2.

The inclusion of the first hydration shell reduces the free energy of ionization by 13.9 – 15.4 eV with respect to the ionization potential of the free Ru^{2+} cation (see Table 3). When two coordination spheres are explicitly included, the corresponding value of $\Delta G_{\mathrm{I}}^{\mathrm{o}}$ is reduced by 18.5 –

20.2 eV relative to the IP of Ru^{2+}. Tables 4 and 5 also give the average and standard deviation of theoretical results within each basis set and each functional category. Free energies predicted by the GGA and MGGA methods are lower than those obtained by the H and HM methods.

As expected, our results indicate that the incorporation of the first and second hydration shells has a large solvent effect on the ionization process. A model such as a combined quantum mechanical and molecular mechanical approach that treats only the bare cation quantum mechanically would be inadequate because of the charge delocalization in the first and second solvation shells. To examine this effect, we calculated the extent of this delocalization using Löwdin population analysis.[89] Since population analysis is most meaningful for small basis sets, we use the smallest basis set (LANL2DZ) for this purpose. The partial atomic charges are reported in Table S1 in the Supporting Information section. When averaged over all density functionals, these population analyses show an average partial charge on Ru(II) of +0.50 (n = 6) and +0.36 (n = 18) and average partial charges on Ru(III) of +0.93 (n = 6) and +0.78 (n = 18). Thus, most of the positive charge is delocalized onto the water molecules of the clusters. The general trend in the charges may be illustrated by the MPWB1K results, which are given in Table 6.

The quality of DFT predictions for the free energy of ionization of the gas-phase $[Ru(H_2O)_n]^{2+}$ complexes cannot be evaluated by comparison with experimental data because such data are not available. However, the validity of the DFT predictions can be examined by comparison of these results to the corresponding values obtained by WFT methods. We performed single-point energy calculations of the $[Ru(H_2O)_n]^{q+}$ clusters (n = 6, 18; q = 2, 3) using the Hartree-Fock (HF) method and second-order Møller-Plesset perturbation theory with the TZQ basis set at the geometries optimized with the MPWB1K/MWB28 level of theory. Table 7 shows calculated adiabatic ionization potentials (I_e) of the $[Ru(H_2O)_n]^{2+}$ clusters as well as ionization potentials corresponding to the low-spin cations ^{1}S Ru^{2+} and ^{2}D Ru^{3+}; the latter have the same metal orbital occupations as the ruthenium-water clusters. In relation to the HF results, the MP2 ionization potentials are increased by 3.6, 3.8,

and 1.9% for ^{1}S Ru^{2+}, $[Ru(H_2O)_6]^{2+}$, and $[Ru(H_2O)_{18}]^{2+}$, respectively. Thus, the inclusion of electron correlation in the calculation of I_e at least at the MP2/TZQ level is critically important for accuracy.

In order to obtain ΔG_I^o(MP2/TZQ), the values of I_e(MP2/TZQ) = 16.28 and 11.52 eV for $[Ru(H_2O)_6]^{2+}$ and $[Ru(H_2O)_{18}]^{2+}$, respectively, were augmented with the zero-point energy ΔZPE and thermal ΔG_{evr}^o contributions; the values of ΔZPE = –0.064 eV and ΔG_{evr}^o = –0.047 eV for $[Ru(H_2O)_6]^{q+}$ as well as ΔZPE = –0.034 eV and ΔG_{evr}^o = –0.005 eV for $[Ru(H_2O)_{18}]^{q+}$ are mean values found by averaging over all the DFT/MWB28 calculations of harmonic frequencies for the corresponding cluster. The final values of ΔG_I^o(MP2/TZQ) are equal to 16.17 and 11.48 eV, respectively for $[Ru(H_2O)_6]^{2+}$ and $[Ru(H_2O)_{18}]^{2+}$, and these values may be compared to the values from DFT calculations in Tables 4 and 5. The values of ΔG_I^o obtained with hybrid and hybrid meta functionals for $[Ru(H_2O)_6]^{2+}$ (ΔG_I^o = 15.9 – 16.3 eV on average for various basis sets) and for $[Ru(H_2O)_{18}]^{2+}$ (11.2 – 11.6 eV) are in better agreement with the MP2 predictions than the corresponding values obtained with GGA and MGGA functionals; the latter give ΔG_I^o = 15.6 – 15.9 eV for $[Ru(H_2O)_6]^{2+}$ and 10.9 – 11.4 eV for $[Ru(H_2O)_{18}]^{2+}$ on average for various basis sets. One can arrive at the same conclusion making comparison of DFT and MP2 values for adiabatic ionization potentials I_e calculated without the zero-point energy and thermal ΔG_{evr}^o corrections, which are small as shown above.

3.3 Solvation Free Energies

The solvation contributions ($\Delta\Delta G_S^o$, eq 6) to the standard reduction potential of $Ru^{3+}_{(aq)}$ are given in Tables 8 and 9 for n = 6 and n = 18, respectively. The $\Delta\Delta G_S^o$ values are in the range from −10.56 to −10.99 eV if the supersolute includes the first hydration shell (n = 6) and in the range between −6.83 and −7.45 eV when the first and second shells are explicitly included (n = 18). The

values obtained with LANL2DZ tend to be more negative than other values. Tables 8 and 9 also list the average values of $\Delta\Delta G_S^o$ and the standard deviations for each combination of a basis set and a functional type. In comparison with GGA and MGGA, the H and HM functionals predict more negative $\Delta\Delta G_S^o$ values, by ~0.12 eV in the case of n = 6 and by ~0.08 eV in the case of n = 18. Tables S3 and S4 in the Supporting Information section display the total solvation free energies (Table S3) as well as the two components, ΔG_{EP} and G_{CDS} (Table S4), for aqueous complexes in both oxidation states with the first and second coordination spheres explicitly treated. A typical sample of these results is shown in the top four rows of Table 10.

We investigated the role of solvation effects in the calculation of relative energies of different molecular structures. According to the BLYP/MWB28 calculation, the gas-phase T_h symmetry structure of $[Ru(H_2O)_{18}]^{2+}$ is less stable than the S_6 conformation (by 1.15 eV). Solvation effects do not change the order, but they lower the relative energy of the T_h structure to 0.69 eV. The impact of solvation on the stability of other molecular structures is less significant.

3.4 Reduction Potential

The gas-phase data in Tables 4 and 5, the solvation free energies in Tables 8 and 9, and the free energy of the reaction in eq 2 (ΔG_{SHE}^o = –4.28 eV, ref 2) were used to compute the standard reduction potential for the $Ru^{3+}|Ru^{2+}$ redox couple by eq 4. The resulting values of $E^o_{Ru^{3+}|Ru^{2+}}$ are given in Table 11 for the calculations with 6 explicit water molecules and in Table 12 for the calculations with 18 explicit water molecules. We also show average values of $E°$ and standard deviations for each combination of a basis set and type of density functional. The values in Table 11 differ significantly from those in Table 12. Curiously, using the same functional (BLYP) as was used in the grand canonical CPMD study[46,47] yields $E^o_{Ru^{3+}|Ru^{2+}}$ in the range from 0.70 to 0.86 V with n = 6 and from –0.31 to –0.12 V for n = 18. Therefore, the results calculated for the clusters with n = 6 are

much closer to the value[46,47] of $E^{o}_{Ru^{3+}|Ru^{2+}}$ = 0.58 V, even though 32 water molecules were explicitly treated in the grand canonical CPMD study.[46,47]

Generally, in the case of six water molecules explicitly included in the treatment, the GGA and MGGA methods combined with MWB28 predict the experimental value of $E^{o}_{Ru^{3+}|Ru^{2+}}$ = 0.23 ± 0.02 V better than the other methods. When the second hydration shell is included in the cluster model of the ruthenium-water complexes (see Table 12), the tendency presented in Table 11 is inverted, now the H and HM functionals provide slightly more accurate predictions for the reduction potential than the other DFT methods used in the present study, even though the majority of values quoted in Table 12 have the opposite sign in comparison with the sign of the experimental value.[49–51] Thus, when we used a cluster model with the first hydration shell explicitly included, our predictions are overestimated in respect to experiment,[49–51] whereas when the second shell is included our values are underestimated, such as the prediction of the thermochemical driving force is opposite to experiment.

The next step is to analyze some possible sources of theory-experiment discrepancies for the $E^{o}_{Ru^{3+}|Ru^{2+}}$ value. Assuming that the experimental value of $E^{o}_{Ru^{3+}|Ru^{2+}}$ is well-established (0.23 ± 0.02 V, see introduction), two main sources of computational error can be identified: errors in predicting the gas-phase ionization free energies for the ruthenium-water clusters and errors in predicting the free energies of solvation for these complexes. Some insight into the uncertainty in the latter can be gained by means of comparison of the $\Delta\Delta G^{o}_{S}$ values calculated with the use of Solvation Model 6 to the corresponding values calculated using a different solvation model, for instance the Polarizable Continuum Model[111] within the Integral Equation Formalism (IEF-PCM) developed by Tomasi et al.[112] and implemented as the default PCM method in *Gaussian03*.[55] We performed a few IEF-PCM calculations of $\Delta\Delta G^{o}_{S}$ with geometries optimized for the gas-phase ruthenium-water clusters. We used the following models for atomic radii: the united-atom universal force field

topological model,[55] the united-atom Hartree-Fock model (UAHF),[113] and the Bondi atomic radii.[114] Results of the IEF-PCM calculations are compared to the corresponding SM6 values in Table 13. Values of $\Delta\Delta G_S^o$ calculated by IEF-PCM noticeably depend (at least, in the case of n = 6) on the type of atomic radii chosen to calculate both electrostatic and non-electrostatic components of the free energy of solvation. We note that, unlike the IEF-PCM model, the SM6 approach employs a set of atomic radii that depend only on the atomic number of an atom,[52] not on its properties. For instance, the UAHF radius of an atom depends on its hybridization state, connectivity, and formal charge.[113] The PCM values of $\Delta\Delta G_S^o$ are systematically underestimated (~0.5 eV on average) with respect to the SM6 values, except the case of UAHF (n = 6) where there is a large overestimate of $\Delta\Delta G_S^o$ (up to 0.8 eV). The reason why one set of PCM values (UAHF, n = 6) differs from other PCM values by such a large amount is unexplained, whereas the discrepancies of ~0.5 eV are quite understandable for highly ionic species, especially in view of even bigger discrepancies in $\Delta\Delta G_S^o$ obtained by alteration of DFT methods within the same SM6 approach.

The gas-phase ionization free energies ΔG_I^o predicted with the use of various DFT methods, basis sets, and effective core potentials vary from 15.48 eV (G96LYP/MWB28) to 16.76 eV (B3P86/LANL2DZ) in the case of $[Ru(H_2O)_6]^{2+}$ and from 10.55 eV (OLYP/MWB28) to 12.78 eV (VSXC/LANL2DZ) in the case of $[Ru(H_2O)_{18}]^{2+}$ (see Tables 4 and 5, respectively). According to the DFT calculations in this paper, the value of ΔG_I^o should lie in the approximate range of 16.12 ± 0.64 eV (n = 6) and 11.66 ± 1.12 eV (n = 18). The values of ΔG_I^o equal to 16.17 (n = 6) and 11.48 (n = 18) eV calculated by second-order Møller-Plesset perturbation theory with the TZQ basis set may be more reliable than some of the DFT values considered in this study; possible uncertainties of ΔG_I^o (MP2/TZQ) that should be less than 0.64 (n = 6) and 1.12 (n = 18) eV are those caused by the incomplete account of electron correlation in the MP2 total energy calculation, the finite basis set

size, and the use of equilibrium geometries and harmonic frequencies computed at the DFT level of theory.

If one assumes that the values of ΔG_I^o equal the MP2/TZQ values of 16.17 eV for n = 6 and 11.48 eV for n = 18, we predict that the "correct" values of $\Delta\Delta G_S^o$ must equal −11.66 (n = 6) and −6.97 (n = 18) eV in order to have a theoretical value of $E^o_{Ru^{3+}|Ru^{2+}}$ in agreement with the experimental value of 0.23 V. This would indicate that all the calculated $\Delta\Delta G_S^o$ values for the $[Ru(H_2O)_6]^{2+}$ cluster are thus significantly underestimated (by 0.7 – 1.1 eV), whereas the $\Delta\Delta G_S^o$ free energies calculated for the $[Ru(H_2O)_{18}]^{2+}$ cluster are mostly overestimated, but only by 0.48 eV or less. Thus, the explicit inclusion of the second solvation shell in calculation of the solvation energies of the ruthenium cations critically improves accuracy. Compared to SM6, the IEF-PCM model[112] provides slightly worse predictions of $\Delta\Delta G_S^o$ (Table 13) with the exception of the UAHF (n = 6) case that may merit additional investigation.

Using ΔG_I^o (MP2/TZQ) along with the values of $\Delta\Delta G_S^o$ = –10.67 and –7.09 eV, respectively, for n = 6 and n = 18 averaged over all the DFT results at the MWB28 basis level, we predict the following $E^o_{Ru^{3+}|Ru^{2+}}$ magnitudes: 1.22 (n = 6) and 0.11 (n = 18) V. Again, the inclusion of the second solvation shell in the treatment significantly improves agreement of theory and experiment (0.23 ± 0.02 V). The use of $\Delta\Delta G_S^o$ averaged at the LANL2DZ and DZQ basis levels provides less accurate predictions for $E^o_{Ru^{3+}|Ru^{2+}}$ than in the case of MWB28: –0.03 and 0.01 V, respectively for LANL2DZ and DZQ (n = 18).

4. Further Discussion

We have shown that reduction potentials for transition metal-containing redox couples can be calculated by mixed discrete and continuum calculations, although there are unsettlingly large uncertainties in the results. It is important to understand the uncertainties.

In earlier work[52] we had shown that the SM6 solvation model with the mPW1PW density functional and the 6-31+G(d,p) basis set agrees with experiment for 112 singly charged main group cations and anions, including 31 ions clustered to a single water molecule with a mean unsigned error (MUE) of 0.14 eV. A later assessment[52] of the SM6/mPW1PW calculations against reevaluated data for these ions gave an MUE of 0.15 eV when averaged over four basis sets. The SM6/B3LYP calculations averaged over two basis sets also gave an MUE of 0.15 eV. The average value of these 112 solvation free energies is –3.03 eV, so an MUE of 0.15 eV corresponds to a 5% error. Both mPW1PW and B3LYP are density functionals of type H, and Table S3 shows that the mean (averaged over functionals and basis sets) type H solvation free energies for $[Ru(H_2O)_n]^{2+}$ are –8.82 eV (n = 6) and –6.92 eV (n = 18), whereas for $[Ru(H_2O)_n]^{3+}$ they are –19.58 eV (n = 6) and –14.10 eV (n = 18). Since the standard deviations in Table S3 consistently increase as the solvation free energies increase, 5% mean error is a more reasonable expectation than a constant 0.15 eV error. Applying the 5% rule gives 0.44 eV (n = 6) and 0.35 eV (n = 18) for Ru^{2+} and 0.98 eV (n = 6) and 0.70 eV (n = 18) for Ru^{3+}. One might hope that there is some cancellation of errors in computing $\Delta\Delta G_S^o$ from $\Delta G_S^o(O)$ and $\Delta G_S^o(R)$, but in fact the standard deviations in Table 8 and 9 tend to be larger by ~30% on average than those expected for $\Delta G_S^o(O)$. Increasing the $\Delta G_S^o(O)$ expected mean errors by 30% yields 1.3 eV for n = 6 and 0.9 eV for n = 18. These rather pessimistic expectations may in fact be overly pessimistic, but at least they serve as a warning not to be too optimistic.

Another issue meriting consideration is that the computation of the polarization free energy within the generalized Born (GB) approach requires specification of Coulomb radii ρ_X for all elements X. While the Coulomb radii for H and O are defined in SM6, no value has been previously determined for Ru. There are various ways in which this parameter might be estimated. For example,

one might require that the difference in solvation free energies computed for bare Ru^{2+} and Ru^{3+} from the Born formula

$$\Delta G_S^o(\mathrm{Ru}^{q+}) = -\frac{1}{2}\left(1-\frac{1}{\varepsilon}\right)\frac{q^2}{\rho_{\mathrm{Ru}}} \tag{12}$$

where ε is the 298.15 K dielectric constant of water (78.3) and q is the charge of the ion, be the precise amount that provides the correct absolute reduction potential, when added to the experimental ionization potential of Ru^{2+}. Using the experimental reduction potential[49–51] of 0.23 V and the free energy change $\Delta G^o_{\mathrm{SHE}} = -4.28$ eV (ref 2) in the SHE reaction (eq 2) we can find the free energy change of $\Delta G^o_{O|R} = -4.51$ eV (eq 3) for reduction in aqueous solution. With the experimental ionization potential[51,109] of Ru^{2+} (28.47 eV), the differential solvation free energy must be –23.96 eV, which corresponds to a Coulomb radius of 1.48 Å in eq 12. However, the utility of the Born equation for highly charged monatomic ions is questionable, since interactions with the first solvation shell may deviate significantly from that expected for a bulk dielectric continuum.

An alternative approach, originally suggested[115] by Morrison and later evaluated by Bondi,[114] makes use of an empirical relationship between atomic radii and ionization potential. In particular, Bondi noted that using

$$\rho_X = 6.13\ \text{Å}\ (I_0 / \text{eV})^{-1/2} \tag{13}$$

provided reasonably good agreement with atomic radii derived from crystallographic analysis. When eq 13 is used with the first, second, and third ionization potentials[51,109] of Ru, radii of 2.26, 1.50, and 1.15 Å are predicted. As Bondi's analysis was carried out using only first ionization potentials and since the radius does not depend on the charge state in SM6, a value of 2.26 Å is probably the most reasonable radius based on this approach.

The various approaches outlined above do not render unambiguous the selection of the ruthenium Coulomb radius. Fortunately, however, the explicit inclusion of the first solvation shell makes that portion of the GB energy associated with the ruthenium atom substantially less sensitive to

ρ_{Ru}, because the explicit solvent shell(s) displace the dielectric continuum away from the central metal atom. Thus, we elected to set the Ru radius equal to 2 Å. An analysis of the sensitivity of the solvation free energies to this choice is presented in Table 10, where solvation free energies computed using alternative radii of 2.26 Å (from the Bondi approach) and 1.74 Å (being smaller than 2 Å by the same amount that the Bondi radius is larger) are presented. As can be seen, the solvation energies change by 0.05 eV or less for these large changes in radii.

Other potential sources of error in the computational prediction of the standard reduction potential of Ru^{3+} in aqueous solution should be mentioned here. There is a possibility of other chemical processes, such as the formation of dimers in aqueous solution, ligand-exchange reactions, and proton transfer, being coupled to the redox reaction. Proton transfer may in particular be important as triply charged ruthenium-water complexes have been determined to have a pK_a of 2.47.[116]

A recent experimental study[117] of the effect of the structure of water on its dielectric response energy and, therefore, on the ion solvation energy predicted a 0.07 V shift for the redox potential of an ionic species because of water structuring effects not accounted for in a continuum approximation, and it is not clear that our CDS terms can account for this kind of effect.

The treatment of the second hydration shell is especially uncertain because we do not know whether the oxidized and reduced species have different coordination numbers in their second hydration shells. The geometries were optimized only in the gas phase, the entropy associated with including multiple alternative structures for the second hydration shell was omitted, and the third hydration shell was treated as a continuum. For example, in the liquid, there could be significant population of configurations with 11 or 13 water molecules in the second hydration shell, and there are also contributions from configurations that are less symmetrically structured than the one included here. The ΔG^{o}_{evr} values used in the present work are based on a single configuration for each value of *n*. In addition to the uncertainties due to neglecting anharmonicity of low-frequency modes

(mentioned in Section 2), ΔG^{o}_{evr} is also uncertain because we neglect the additional entropy contributions that would come from considering additional conformations. Whereas anharmonicity of low-frequency modes would decrease the calculated entropy, this conformational entropy would increase it; however, there is no reason to think that the two corrections to the harmonic value would be precisely cancelled. For both effects, the critical number is the difference in the effect for q = 2 and q = 3. It is hard to make an estimate of the uncertainty in ΔG^{o}_{evr}, but we will estimate an 0.05 eV uncertainty in this term.

A question that always arises in the treatment of systems containing transition metals is the need to take explicit account of multireference effects. A recent study[118] of the $Fe^{3+}|Fe^{2+}$ reduction potential has employed the complete active space second-order perturbation theory CASPT2 method with a basis set of double-ζ quality to calculate the ionization potential of the $[Fe(H_2O)_6]^{2+}$ cluster, though without the explicit treatment of the second solvation shell and with the geometries being optimized in the gas phase at the MP2 level of theory. The PCM solvation model was used in calculations of solvation energies.[118] The PCM/CASPT2 method provides more accurate prediction of the $Fe^{3+}|Fe^{2+}$ reduction potential in comparison with experiment than those obtained at the PCM/B3LYP level.[118] However B3LYP is not among the preferred functionals for including multireference effects in transition metal systems.[63]

As discussed in Section 3.1, the geometries for the aqua complexes were optimized in the gas phase and show systematically large Ru–O distances. To see the effect of this on the solvation energies, we performed some calculations in which we constrained the Ru–O distances to their liquid-phase values. The results of these calculations are given in Table S2 of the Supporting Information; typically G_{CDS} increases by ~0.02 eV, whereas ΔG_{ENP} typically changes by −0.14 eV for q = 3, n = 6 and by −0.03 to +0.01 eV for the other three cases. The net effect is that ΔG^{o}_{S} typically decreases by −0.11 eV for n = 6 and by −0.03 eV for n = 18. The larger change for n = 6 is significant and is in the correct direction to correct the systematic error in the value of the reduction potential at n = 6.

Finally, we consider the effect of the atomic surface tension of Ru. Since, as discussed in Section 2, the ruthenium atom has very little solvent accessible surface area in the water complexes, and the magnitude of a typical atomic surface tension is about 0.004 eV,[52] the effect can be estimated to be 0.01 eV or smaller and is negligible.

5. Conclusions

We have presented a detailed computational study of the aqueous reduction potential of the $Ru^{3+}|Ru^{2+}$ redox couple. We employed exchange-correlation functionals classified into four categories (GGA, H, MGGA, and HM) combined with five ECPs and basis sets (each basis set includes an ECP definition). The solvation free energy is calculated by the SM6 continuum solvation model that accounts for long-ranged bulk electrostatics as well as for non-electrostatic cavitation, dispersion, and solvent-structure effects. We carried out calculations of the ruthenium-water clusters $[Ru(H_2O)_n]^{q+}$ (q = 2, 3), either the first (n = 6) or the first two (n = 18) hydration shells being explicitly treated. This computational protocol is based on a thermodynamic cycle where the electrochemical parameter is determined by the ionization free energy, the solvation free energy of the oxidized and reduced redox states, and the experimental free energy for the standard hydrogen electrode.

The reduction potential $E^{o}_{Ru^{3+}|Ru^{2+}}$ is overestimated when only the first coordination shell is treated explicitly whereas it is underestimated when the first two hydration shells are considered in the cluster model. The inclusion of the second solvation shell is important for the accuracy of theoretical predictions of the solvation free energy and the standard potential for reduction of the Ru^{3+} cation in aqueous solution. We observed that hybrid and hybrid meta functionals provide the most accurate geometries and ionization potentials for the ruthenium-water complexes, and possibly they also provide more accurate predictions of the standard reduction potential $E^{o}_{Ru^{3+}|Ru^{2+}}$ than those obtained using other types of functionals. However, due to large uncertainties in the numbers calculated using different density functionals, basis sets, and effective core potentials, it is impossible

to identify the most reliable computational method for calculating the standard reduction potential of $Ru^{3+}|Ru^{2+}$ and other redox couples. It is clearly dangerous to rely on theoretical predictions obtained within any single DFT method (see refs 46 and 47, for an example of such calculations).

Although some of the calculations agree quite well with experiment, the extensive documentation of the sensitivity of $E^{o}_{O|R}$ to density functionals, basis sets, effective core potentials, solvation modeling protocols, and calculated ionization potentials comprises a meta-analysis that quantifies the sources of uncertainty in the calculation of redox potentials of transition metals and other species, and this may help guide the course of future theoretical studies.

Acknowledgments. The authors are grateful to Casey Kelly and Jingjing Zheng for helpful assistance. This work was supported by the Office of Naval Research under award no. N00014-05-1-0538.

Supporting Information Available: Partial atomic charges (Löwdin population analysis) on Ru and water molecules in the ruthenium-water complexes ($[Ru(H_2O)_n]^{q+}$; n = 6, 18; q = 2, 3); solvation free energies for optimized gas-phase complexes and for partially optimized aqueous complexes; solvation free energies of individual clusters; values of the ΔG_{EP} and G_{CDS} components of the solvation free energy. This material is available free of charge via the Internet as a link associated with the manuscript.

References

(1) Wardman, P. *J. Phys. Chem. Ref. Data* **1989**, *18*, 1637.

(2) Kelly, C. P.; Cramer, C. J.; Truhlar, D. G. *J. Phys. Chem. B* **2006**, *110*, 16066.

(3) Lewis, A.; Bumpus, J. A.; Truhlar, D. G.; Cramer, C. J. *J. Chem. Ed.* **2004**, *81*, 596; and erratum in press.

(4) Winget, P.; Weber, E. J.; Cramer, C. J.; Truhlar, D. G. *Phys. Chem. Chem. Phys.* **2000**, *2*, 1231.

(5) Patterson, E. V.; Cramer, C. J.; Truhlar, D. G. *J. Am Chem. Soc.* **2001**, *123*, 2025.

(6) Winget, P.; Cramer, C. J.; Truhlar, D. G. *Theor. Chem. Acc.* **2004**, *112*, 217.

(7) Reynolds, C. A.; King, P. M.; Richards, W. G. *J. Chem. Soc., Chem. Commun.* **1988**, 1434.

(8) Reynolds, C. A.; King, P. M.; Richards, W. G. *Nature* **1988**, *334*, 80.

(9) Lister, S. G.; Reynolds, C. A.; Richards, W. G. *Int. J. Quantum Chem.* **1992**, *41*, 293.

(10) Wolfe, J. J.; Wright, J. D.; Reynolds, C. A.; Saunders, A. C. G. *Anti-Cancer Drug Des.* **1994**, *9*, 85.

(11) Reynolds, C. A. *Int. J. Quantum Chem.* **1995**, *56*, 677.

(12) Boesch, S. E.; Grafton, A. K.; Wheeler, R. A. *J. Phys. Chem.* **1996**, *100*, 10083.

(13) Raymond, K. S.; Grafton, A. K.; Wheeler, R. A. *J. Phys. Chem. B* **1997**, *101*, 623.

(14) Kettle, L. J.; Bates, S. P.; Mount, A. R. *Phys. Chem. Chem. Phys.* **2000**, *2*, 195.

(15) Kaszynski, P. *J. Phys. Chem. A* **2001**, *105*, 7626.

(16) Fabre, B.; Hapiot, P.; Simonet, J. *J. Phys. Chem. A* **2002**, *106*, 5422.

(17) Fontanesi, C.; Benassi, R.; Giovanardi, R.; Marcaccio, M.; Paolucci, F.; Roffia, S. *J. Mol. Struct.* **2002**, *612*, 277.

(18) Baik, M.-H.; Friesner, R. A. *J. Phys. Chem. A* **2002**, *106*, 7407.

(19) Baik, M.-H.; Schauer, C. K.; Ziegler, T. *J. Am. Chem. Soc.* **2002**, *124*, 11167.

(20) Namazian, M.; Norouzi, P.; Ranjbar, R. *J. Mol. Struct.* (*Theochem*) **2003**, *625*, 235.

(21) Namazian, M. *J. Mol. Struct.* (*Theochem*) **2003**, *664-665*, 273.

(22) Benassi, R.; Ferrarini, P.; Fontanesi, C.; Benedetti, L.; Paolucci, F. *J. Electroanal. Chem.* **2004**, *564*, 231.

(23) Namazian, M.; Almodarresieh, H. A. *J. Mol. Struct.* (*Theochem*) **2004**, *686*, 97.

(24) Fu, Y.; Liu, L.; Yu, H.-Z.; Wang, Y.-M.; Guo, Q.-X. *J. Am. Chem. Soc.* **2005**, *127*, 7227.

(25) Dutton, A. S.; Fukuto, J. M.; Houk, K. N. *Inorg. Chem.* **2005**, *44*, 4024.

(26) Camurri, G.; Ferrarini, P.; Giovanardi, R.; Benassi, R.; Fontanesi, C. *J. Electroanal. Chem.* **2005**, *585*, 181.

(27) Shamsipur, M.; Alizadeh, K.; Arshadi, S. *J. Mol. Struct.* (*Theochem*) **2006**, *758*, 71.

(28) Wass, J. R. T. J.; Ahlberg, E.; Panas, I.; Schiffrin, D. J. *J. Phys. Chem. A* **2006**, *110*, 2005.

(29) Bottoni, A.; Cosimelli, B.; Scavetta, E.; Spinelli, D.; Spisani, R.; Stenta, M.; Tonelli, D. *Mol. Phys.* **2006**, *104*, 2961.

(30) Li, J.; Fisher, C. L.; Chen, J. L.; Bashford, D.; Noodleman, L. *Inorg. Chem.* **1996**, *35*, 4694.

(31) Becke, A. D. *Phys. Rev. A* **1988**, *38*, 3098.

(32) Perdew, J. P. *Phys. Rev. B* **1986**, *33*, 8822.

(33) Uudsemaa, M.; Tamm, T. *J. Phys. Chem. A* **2003**, *107*, 9997.

(34) Bratsch, S. G. *J. Phys. Chem. Ref. Data* **1989**, *18*, 1.

(35) Uudsemaa, M.; Tamm, T. *Chem. Phys. Lett.* **2001**, *342*, 667.

(36) Uudsemaa, M.; Tamm, T. *Chem. Phys. Lett.* **2004**, *400*, 54.

(37) Pavlov, M.; Siegbahn, P. E. M.; Sandström, M. *J. Phys. Chem. A* **1998**, *102*, 219.

(38) Pye, C. C.; Rudolph, W. W. *J. Phys. Chem. A* **1998**, *102*, 9933.

(39) Markham, G. D.; Glusker, J. P.; Bock, C. W. *J. Phys. Chem. B* **2002**, *106*, 5118.

(40) Bock, C. W.; Markham, G. D.; Katz, A. K.; Glusker, J. P. *Inorg. Chem.* **2003**, *42*, 1538.

(41) Holland, J. P.; Green, J. C.; Dilworth, J. R. *Dalton Trans.* **2006**, 783.

(42) Tavernelli, I.; Vuilleumier, R.; Sprik, M. *Phys. Rev. Lett.* **2002**, *88*, 213002-1.

(43) Car, R.; Parrinello, M. *Phys. Rev. Lett.* **1985**, *55*, 2471.

(44) Blumberger, J.; Bernasconi, L.; Tavernelli, I.; Vuilleumier, R.; Sprik, M. *J. Am. Chem. Soc.* **2004**, *126*, 3928.

(45) Blumberger, J.; Sprik, M. *J. Phys. Chem. B* **2004**, *108*, 6529.

(46) Blumberger, J.; Sprik, M. *J. Phys. Chem. B* **2005**, *109*, 6793.

(47) Blumberger, J.; Sprik, M. *Theor. Chem. Acc.* **2006**, *115*, 113.

(48) Tateyama, Y.; Blumberger, J.; Sprik, M.; Tavernelli, I. *J. Chem. Phys.* **2005**, *122*, 234505-1.

(49) Mercer, E. E.; Buckley, R. R. *Inorg. Chem.* **1965**, *4*, 1692.

(50) Buckley, R. R; Mercer, E. E. *J. Phys. Chem.* **1966**, *70*, 3103. Milazzo, G.; Caroli, S.; Sharma, V. K. *Tables of Standard Electrode Potentials*; Wiley: Chichester, 1978. Bard, A. J.; Parsons, R.; Jordan, J. *Standard Potentials in Aqueous Solutions*; Marcel Dekker: New York, 1985.

(51) Vanýsek, P. In *CRC Handbook of Chemistry and Physics*; Lide, D. R., Ed.; 87th edition; CRC Taylor and Francis: Boca Raton, 2006; pages 8-24 and 8-26.

(52) Kelly, C. P.; Cramer, C. J.; Truhlar, D. G. *J. Chem. Theory Comput.* **2005**, *1*, 1133.

(53) Zhu, T.; Li, J.; Hawkins, G. D.; Cramer, C. J.; Truhlar, D. G. *J. Chem. Phys.* **1998**, *109*, 9117; **2000**, *113*, 3930 (E).

(54) Giesen, D. J.; Storer, J. W.; Cramer, C. J.; Truhlar, D. G. *J. Am. Chem. Soc.* **1995**, *117*, 1057. Chambers, C. C.; Hawkins, G. D.; Cramer, C. J.; Truhlar, D. G. *J. Phys. Chem.* **1996**, *100*, 16385.

(55) Frisch, M. J.; Trucks, G. W.; Schlegel, H. B.; Scuseria, G. E.; Robb, M. A.; Cheeseman, J. R.; Montgomery, Jr., J. A.; Vreven, T.; Kudin, K. N.; Burant, J. C.; Millam, J. M.; Iyengar, S. S.; Tomasi, J.; Barone, V.; Mennucci, B.; Cossi, M.; Scalmani, G.; Rega, N.; Petersson, G. A.; Nakatsuji, H.; Hada, M.; Ehara, M.; Toyota, K.; Fukuda, R.; Hasegawa, J.; Ishida, M.; Nakajima, T.; Honda, Y.; Kitao, O.; Nakai, H.; Klene, M.; Li, X.; Knox, J. E.; Hratchian, H. P.; Cross, J. B.; Bakken, V.; Adamo, C.; Jaramillo, J.; Gomperts, R.; Stratmann, R. E.; Yazyev, O.; Austin, A. J.; Cammi, R.; Pomelli, C.; Ochterski, J. W.; Ayala, P. Y.; Morokuma, K.; Voth, G. A.; Salvador, P.; Dannenberg, J. J.; Zakrzewski, V. G.; Dapprich, S.; Daniels, A. D.; Strain, M. C.; Farkas, O.; Malick, D. K.; Rabuck, A. D.; Raghavachari, K.; Foresman, J. B.; Ortiz, J. V.; Cui, Q.; Baboul, A. G.; Clifford, S.; Cioslowski, J.; Stefanov, B. B.; Liu, G.; Liashenko, A.; Piskorz, P.; Komaromi, I.; Martin, R. L.; Fox, D. J.; Keith, T.; Al-Laham, M. A.; Peng, C. Y.; Nanayakkara, A.; Challacombe, M.; Gill, P. M. W.; Johnson, B.; Chen, W.; Wong, M. W.; Gonzalez, C.; Pople, J. A. *Gaussian 03, Revision C.02*; Gaussian, Inc.: Wallingford, CT, 2004.

(56) Hay, P. J.; Wadt, W. R. *J. Chem. Phys.* **1985**, *82*, 270.

(57) Stevens, W. J.; Basch, H.; Krauss, M. *J. Chem. Phys.* **1984**, *81*, 6026. Stevens, W. J.; Krauss, M.; Basch, H.; Jasien, P. G. *Can. J. Chem.* **1992**, *70*, 612.

(58) Schultz, N. E.; Zhao, Y.; Truhlar, D. G. *J. Phys. Chem. A* **2005**, *109*, 4388; see also http://comp.chem.umn.edu/basissets/basis.cgi

(59) Andrae, D.; Häußermann, U.; Dolg, M.; Stoll, H.; Preuß, H. *Theor. Chim. Acta* **1990**, *77*, 123.

(60) Hariharan, P. C.; Pople, J. A. *Theor. Chim. Acta* **1973**, *28*, 213.

(61) Lynch, B. J.; Zhao, Y.; Truhlar, D. G. *J. Phys. Chem. A* **2003**, *107*, 1384.

(62) Curtiss, L. A.; Raghavachari, K.; Redfern, P. C.; Rassolov, V.; Pople, J. A. *J. Chem. Phys.* **1998**, *109*, 7764. Fast, P. L.; Sánchez, M. L.; Truhlar, D. G. *Chem. Phys. Lett.* **1999**, *306*, 407.

(63) Schultz, N. E.; Zhao, Y.; Truhlar, D. G. *J. Phys. Chem. A* **2005**, *109*, 11127.

(64) Lee, C.; Yang, W.; Parr, R. G. *Phys. Rev. B* **1988**, *37*, 785.

(65) Perdew, J. P.; Burke, K.; Ernzerhof, M. *Phys. Rev. Lett.* **1996**, *77*, 3865.

(66) Perdew, J. P. In *Electronic Structure of Solids*; Ziesche, P., Eschrig, H., Eds.; Akademie Verlag: Berlin, Germany, 1991; p. 11.

(67) Gill, P. M. W. *Mol. Phys.* **1996**, *89*, 433.

(68) Hamprecht, F. A.; Cohen, A. J.; Tozer, D. J.; Handy, N. C. *J. Chem. Phys.* **1998**, *109*, 6264.

(69) Adamo, C.; Barone, V. *J. Chem. Phys.* **1998**, *108*, 664.

(70) Handy, N. C.; Cohen, A. J. *Mol. Phys.* **2001**, *99*, 403.

(71) Stephens, P. J.; Devlin, F. J.; Chabalowski, C. F.; Frisch, M. J. *J. Phys. Chem.* **1994**, *98*, 11623.

(72) Becke, A. D. *J. Chem. Phys.* **1993**, *98*, 5648.

(73) Wilson, P. J.; Bradley, T. J.; Tozer, D. J. *J. Chem. Phys.* **2001**, *115*, 9233.

(74) Schmider, H. L.; Becke, A. D. *J. Chem. Phys.* **1998**, *108*, 9624.

(75) Hoe, W.-M.; Cohen, A. J.; Handy, N. C. *Chem. Phys. Lett.* **2001**, *341*, 319.

(76) Adamo, C.; Cossi, M.; Barone, V. *J. Mol. Struct.* (*Theochem*) **1999**, *493*, 145.

(77) Ernzerhof, M.; Scuseria, G. E. *J. Chem. Phys.* **1999**, *110*, 5029.

(78) Becke, A. D. *J. Chem. Phys.* **1996**, *104*, 1040.

(79) Krieger, J. B.; Chen, J.; Iafrate, G. J.; Savin, A. In *Electron Correlations and Materials Properties*; Gonis, A., Kioussis, N., Ciftan, M., Eds.; Plenum: New York, 1999; p. 463.

(80) Zhao, Y.; González-García, N.; Truhlar, D. G. *J. Phys. Chem. A* **2005**, *109*, 2012.

(81) Tao, J.; Perdew, J. P.; Staroverov, V. N.; Scuseria, G. E. *Phys. Rev. Lett.* **2003**, *91*, 146401-1.

(82) Voorhis, T. V.; Scuseria, G. E. *J. Chem. Phys.* **1998**, *109*, 400.

(83) Zhao, Y.; Truhlar, D. G. *J. Chem. Theory Comput.* **2005**, *1*, 415.

(84) Staroverov, V. N.; Scuseria, G. E.; Tao, J.; Perdew, J. P. *J. Chem. Phys.* **2003**, *119*, 12129.

(85) Staroverov, V. N.; Scuseria, G. E.; Tao, J.; Perdew, J. P. *J. Chem. Phys.* **2004**, *121*, 11507 (E).

(86) Bartmess, J. E. *J. Phys. Chem.* **1994**, *98*, 6420.

(87) Basolo, F.; Pearson, R. G. *Mechanisms of Inorganic Reactions; a Study of Metal Complexes in Solution*; Wiley: New York, 1967.

(88) Cramer, C. J.; Truhlar, D. G. In *Solvent Effects and Chemical Reactivity*; Tapia, O., Bertran, J., Eds.; Kluwer: Dordrecht, 1996; p. 1.

(89) Löwdin, P.-O. *J. Chem. Phys.* **1950**, *18*, 365.

(90) Chamberlin, A. C.; Kelly, C. P.; Thompson, J. D.; Xidos, J. D.; Li, J.; Hawkins, G. D.; Winget, P.; Zhu, T.; Rinaldi, D.; Liotard, D. A.; Cramer, C. J.; Truhlar, D. G.; Frisch, M. J. *MN-GSM, version 6.0*; University of Minnesota, Minneapolis, MN 55455-0431, 2006.

(91) Møller, C.; Plesset, M. S. *Phys. Rev*. **1934**, *46*, 618.

(92) Head-Gordon, M.; Pople, J. A.; Frisch, M. J. *Chem. Phys. Lett.* **1988**, *153*, 503.

(93) Purvis, G. D., III; Bartlett, R. J. *J. Chem. Phys.* **1982**, *76*, 1910.

(94) Raghavachari, K.; Trucks, G. W.; Pople, J. A.; Head-Gordon, M. *Chem. Phys. Lett.* **1989**, *157*, 479.

(95) Noga, J.; Bartlett, R. J. *J. Chem. Phys.* **1987**, *86*, 7041.

(96) Stanton, J. F.; Gauss, J.; Watts, J. D.; Lauderdale, W. J.; Bartlett, R. J. *Int. J. Quantum Chem.: Quantum Chem. Symp.* **1992**, *26*, 879.

(97) Schmidt, M. W.; Baldridge, K. K.; Boatz, J. A.; Elbert, S. T.; Gordon, M. S.; Jensen, J. H.; Koseki, S.; Matsunaga, N.; Nguyen, K. A.; Su, S.; Windus, T. L.; Dupuis, M.; Montgomery, J. A., Jr. *J. Comput. Chem.* **1993**, *14*, 1347.

(98) Fedorov, D. G.; Koseki, S.; Schmidt, M. W.; Gordon, M. S. *Int. Rev. Phys. Chem.* **2003**, *22*, 551.

(99) Greenwood, N. N.; Earnshaw, A. *Chemistry of the Elements*; 2nd edition; Butterworth-Heinemann: Boston, MA, 1997.

(100) Richens, D. T. *The Chemistry of Aqua Ions*; John Wiley & Sons: New York, 1997.

(101) Åkesson, R.; Pettersson, L. G. M.; Sandström, M.; Wahlgren, U. *J. Am. Chem. Soc.* **1994**, *116*, 8691.

(102) Rosso, K. M.; Rustad, J. R.; Gibbs, G. V. *J. Phys. Chem. A* **2002**, *106*, 8133.

(103) Ohtaki, H.; Radnai, T. *Chem. Rev.* **1993**, *93*, 1157.

(104) Jahn, H. A.; Teller, E. *Proc. R. Soc. London A* **1937**, *161*, 220.

(105) Brunschwig, B. S.; Creutz, C.; Macartney, D. H.; Sham, T.-K.; Sutin, N. *Faraday Discuss. Chem. Soc.* **1982**, *74*, 113.

(106) Marcos, E. S.; Pappalardo, R. R.; Rinaldi, D. *J. Phys. Chem.* **1991**, *95*, 8928.

(107) Troullier, N.; Martins, J. L. *Phys. Rev. B* **1991**, *43*, 1993.

(108) Bock, C. W.; Markham, G. D.; Katz, A. K.; Glusker, J. P. *Theor. Chem. Acc.* **2006**, *115*, 100.

(109) Moore, C. E. *Atomic Energy Levels as Derived from the Analyses of Optical Spectra*; NSRDS-NBS 35, Volume III: Washington, D.C., 1971.

(110) Godbout, N.; Salahub, D. R.; Andzelm, J.; Wimmer, E. *Can. J. Chem.* **1992**, *70*, 560.

(111) Miertuš, S.; Scrocco, E.; Tomasi, J. *Chem. Phys.* **1981**, *55*, 117.

(112) Tomasi, J.; Mennucci, B.; Cancès, E. *J. Mol. Struct.* (*Theochem*) **1999**, *464*, 211.

(113) Barone, V.; Cossi, M.; Tomasi, J. *J. Chem. Phys.* **1997**, *107*, 3210.

(114) Bondi, A., *J. Phys. Chem.* **1964**, *68*, 441.

(115) Morrison, J. D. *Rev. Pure Appl. Chem.* **1955**, *5*, 22.

(116) Stebler-Röthlisberger, M.; Hummel, W.; Pittet, P.-A.; Bürgi, H.-B.; Ludi, A.; Merbach, A. E. *Inorg. Chem.* **1988**, *27*, 1358.

(117) Khanova, L. A.; Topolev, V. V.; Krishtalik, L. I. *Chem. Phys.* **2006**, *326*, 33.

(118) Tsushima, S.; Wahlgren, U.; Grenthe, I. *J. Phys. Chem. A* **2006**, *110*, 9175.

TABLE 1: Average Ru–O Distances (in Å) in the Gas-Phase Clusters $[Ru(H_2O)_6]^{q+}$ (q = 2, 3) of C_i Symmetry [a]

Method	LANL2DZ		DZQ		MWB28		TZQ		*AMUE* [b]
	Ru^{2+}	Ru^{3+}	Ru^{2+}	Ru^{3+}	Ru^{2+}	Ru^{3+}	Ru^{2+}	Ru^{3+}	
GGA									
BLYP	2.188	2.120	2.192	2.126	2.174	2.109	2.181	2.110	0.080
BP86	2.159	2.095	2.164	2.102	2.146	2.086	2.151	2.085	0.054
BPBE	2.161	2.097	2.167	2.104	2.149	2.087	2.153	2.086	0.055
BPW91	2.164	2.099	2.169	2.106	2.151	2.089	2.156	2.088	0.059
G96LYP	2.180	2.113	2.186	2.120	2.166	2.103	2.174	2.104	0.073
HCTH	2.182	2.107	2.187	2.113	2.167	2.094	2.171	2.092	0.069
mPWLYP	2.183	2.117	2.188	2.123	2.170	2.106	2.176	2.107	0.076
mPWPBE	2.157	2.094	2.162	2.101	2.144	2.084	2.149	2.083	0.052
mPWPW	2.160	2.096	2.165	2.103	2.147	2.086	2.151	2.085	0.054
OLYP	2.186	2.115	2.191	2.120	2.17	2.101	2.175	2.099	0.075
PBE	2.159	2.095	2.164	2.102	2.146	2.085	2.150	2.084	0.053
AUE [c]	0.061	0.074	0.066	0.081	0.047	0.064	0.052	0.063	
H									
B3LYP	2.163	2.090	2.172	2.099	2.155	2.084	2.159	2.082	0.055
B3P86	2.136	2.068	2.146	2.078	2.129	2.063	2.132	2.062	0.032
B3PW91	2.146	2.075	2.155	2.084	2.138	2.070	2.141	2.068	0.040
B97-1	2.158	2.088	2.169	2.098	2.150	2.084	2.154	2.081	0.053
B97-2	2.153	2.077	2.164	2.089	2.146	2.074	2.149	2.070	0.045
B98	2.154	2.085	2.164	2.095	2.146	2.081	2.150	2.078	0.049
BH&HLYP	2.154	2.071	2.164	2.084	2.146	2.070	2.149	2.067	0.043
mPW1PW	2.140	2.067	2.150	2.079	2.133	2.065	2.135	2.061	0.034
O3LYP	2.167	2.093	2.177	2.103	2.158	2.087	2.161	2.083	0.059
PBEh	2.139	2.068	2.149	2.078	2.131	2.064	2.133	2.060	0.033
AUE [c]	0.041	0.048	0.051	0.059	0.033	0.044	0.036	0.041	

TABLE 1: Continued

MGGA									
BB95	2.168	2.103	2.173	2.110	2.154	2.091	2.159	2.091	0.061
mPWB95	2.164	2.100	2.169	2.106	2.151	2.088	2.155	2.088	0.058
mPWKCIS	2.174	2.108	2.178	2.113	2.160	2.097	2.165	2.096	0.066
PBEKCIS	2.175	2.109	2.180	2.115	2.161	2.098	2.166	2.097	0.068
TPSSKCIS	2.161	2.097	2.167	2.104	2.149	2.088	2.154	2.088	0.056
TPSS	2.151	2.089	2.157	2.096	2.139	2.081	2.144	2.080	0.047
VSXC	2.199	2.115	2.205	2.121	2.181	2.101	2.193	2.105	0.083
AUE [c]	0.063	0.073	0.066	0.079	0.046	0.062	0.052	0.062	
HM									
B1B95	2.146	2.071	2.155	2.081	2.138	2.066	2.140	2.063	0.038
BB1K	2.140	2.058	2.149	2.072	2.132	2.057	2.133	2.053	0.029
MPW1B95	2.142	2.066	2.151	2.076	2.134	2.062	2.136	2.058	0.033
MPW1KCIS	2.158	2.087	2.168	2.098	2.150	2.082	2.153	2.080	0.052
MPWKCIS1K	2.145	2.064	2.155	2.077	2.138	2.064	2.139	2.059	0.035
PBE1KCIS	2.155	2.081	2.165	2.092	2.147	2.078	2.150	2.074	0.048
MPWB1K	2.137	2.056	2.146	2.069	2.130	2.054	2.130	2.050	0.026
TPSS1KCIS	2.150	2.082	2.160	2.091	2.143	2.077	2.146	2.075	0.045
TPSSh	2.142	2.077	2.152	2.087	2.134	2.072	2.138	2.070	0.039
AUE [c]	0.036	0.041	0.046	0.053	0.028	0.038	0.031	0.035	
Experiment (ref 105)							2.110	2.030	
CPMD Calculation (refs 46 and 47)							2.180	2.100	

[a] Results of the TZQS calculations are omitted; they are identical to those at TZQ within 0.001 Å.

[b] The mean unsigned error (MUE) is a theory-experiment deviation averaged for both oxidation states (+2 and +3); the values of MUE averaged over all the basis sets are calculated as AMUE = [MUE(LANL2DZ) + MUE(DZQ) + MUE(MWB28) + MUE(TZQ)]/4.

[c] Theory-experiment deviations averaged over all the functionals of this category.

TABLE 2: Ru–O Distances (in Å) in the First Coordination Shell of the Gas-Phase Clusters $[Ru(H_2O)_{18}]^{q+}$ (q = 2, 3) of S_6 Symmetry [a]

Method	LANL2DZ		DZQ		MWB28		TZQ		*AMUE* [b]
	Ru^{2+}	Ru^{3+}	Ru^{2+}	Ru^{3+}	Ru^{2+}	Ru^{3+}	Ru^{2+}	Ru^{3+}	
GGA									
BLYP	2.189	2.097	2.192	2.103	2.175	2.089	2.181	2.088	0.069
BP86	2.162	2.074	2.165	2.080	2.149	2.066	2.151	2.064	0.044
BPBE	2.164	2.076	2.167	2.082	2.151	2.068	2.154	2.065	0.046
BPW91	2.167	2.078	2.169	2.084	2.153	2.069	2.156	2.068	0.048
G96LYP	2.180	2.090	2.183	2.096	2.166	2.081	2.171	2.081	0.061
HCTH	2.183	2.083	2.186	2.090	2.169	2.073	2.172	2.068	0.058
mPWLYP	2.186	2.096	2.188	2.101	2.172	2.087	2.177	2.086	0.067
mPWPBE	2.161	2.074	2.164	2.080	2.148	2.065	2.150	2.063	0.043
mPWPW	2.163	2.076	2.166	2.082	2.150	2.067	2.153	2.065	0.045
OLYP	2.186	2.086	2.190	2.091	2.171	2.075	2.175	2.072	0.061
PBE	2.163	2.075	2.166	2.081	2.150	2.067	2.152	2.064	0.045
AUE [c]	0.063	0.052	0.066	0.058	0.049	0.043	0.053	0.041	
H									
B3LYP	2.161	2.068	2.169	2.078	2.153	2.065	2.156	2.062	0.044
B3P86	2.136	2.047	2.143	2.057	2.128	2.044	2.129	2.041	0.021
B3PW91	2.144	2.054	2.152	2.064	2.136	2.051	2.138	2.047	0.028
B97-1	2.156	2.070	2.165	2.079	2.148	2.066	2.151	2.062	0.042
B97-2	2.152	2.055	2.160	2.066	2.144	2.053	2.146	2.049	0.033
B98	2.152	2.067	2.161	2.076	2.144	2.063	2.147	2.059	0.039
BH&HLYP	2.148	2.049	2.157	2.061	2.141	2.048	2.143	2.044	0.029
mPW1PW	2.139	2.048	2.147	2.059	2.131	2.046	2.132	2.042	0.023
O3LYP	2.167	2.067	2.175	2.077	2.157	2.062	2.160	2.058	0.045
PBEh	2.138	2.047	2.146	2.058	2.130	2.045	2.131	2.041	0.022
AUE [c]	0.039	0.027	0.047	0.038	0.031	0.024	0.033	0.021	

TABLE 2: Continued

MGGA									
BB95	2.171	2.079	2.173	2.086	2.156	2.069	2.158	2.066	0.050
mPWB95	2.168	2.077	2.170	2.083	2.154	2.068	2.155	2.065	0.048
mPWKCIS	2.177	2.086	2.179	2.092	2.163	2.077	2.166	2.075	0.057
PBEKCIS	2.179	2.088	2.181	2.093	2.165	2.078	2.168	2.076	0.059
TPSSKCIS	2.165	2.077	2.168	2.083	2.152	2.069	2.156	2.068	0.047
TPSS	2.155	2.069	2.158	2.076	2.142	2.062	2.145	2.060	0.038
VSXC	2.211	2.117	2.217	2.122	2.194	2.102	2.207	2.108	0.090
AUE [c]	0.065	0.055	0.068	0.061	0.051	0.045	0.055	0.044	
HM									
B1B95	2.143	2.046	2.150	2.057	2.135	2.043	2.133	2.040	0.023
BB1K	2.136	2.035	2.143	2.047	2.129	2.034	2.128	2.030	0.015
MPW1B95	2.139	2.042	2.146	2.054	2.132	2.039	2.132	2.036	0.020
MPW1KCIS	2.158	2.067	2.166	2.076	2.150	2.062	2.152	2.059	0.041
MPWKCIS1K	2.141	2.044	2.150	2.056	2.134	2.043	2.135	2.038	0.023
PBE1KCIS	2.154	2.061	2.162	2.071	2.146	2.057	2.148	2.053	0.037
MPWB1K	2.133	2.033	2.140	2.045	2.126	2.031	2.126	2.028	0.013
TPSS1KCIS	2.151	2.062	2.159	2.072	2.143	2.058	2.146	2.056	0.036
TPSSh	2.144	2.058	2.151	2.067	2.135	2.054	2.138	2.051	0.030
AUE [c]	0.034	0.020	0.042	0.031	0.027	0.017	0.028	0.013	
Experiment (ref 105)							2.110	2.030	
CPMD Calculation (refs 46 and 47)							2.180	2.100	

[a] Geometry optimization of the $[Ru(H_2O)_{18}]^{3+}$ cluster at the TZQS level was performed using only GGA and MGGA type functionals. Results of these TZQS calculations are omitted; they are identical to those at TZQ within 0.001 Å.

[b, c] See footnotes to Table 1

TABLE 3: Third Ionization Potential (in eV) of the Bare Ruthenium Atom [a]

Method	LANL2DZ	DZQ	MWB28	TZQ	Method	LANL2DZ	DZQ	MWB28	TZQ
GGA					**H**				
BLYP	29.25	28.87	28.84	28.92	B3LYP	29.25	28.88	28.85	28.93
BP86	29.37	29.03	28.94	29.07	B3P86	29.76	29.43	29.35	29.47
BPBE	29.19	28.82	28.73	28.86	B3PW91	29.12	28.76	28.68	28.80
BPW91	29.22	28.85	28.76	28.89	B97-1	29.24	28.85	28.81	28.90
G96LYP	29.17	28.83	28.76	28.87	B97-2	29.24	28.80	28.82	28.84
HCTH	29.48	29.06	29.13	29.09	B98	29.28	28.90	28.84	28.94
mPWLYP	29.31	28.92	28.90	28.96	BH&HLYP	28.82	28.45	28.44	28.51
mPWPBE	29.25	28.86	28.79	28.90	mPW1PW	29.06	28.67	28.61	28.72
mPWPW	29.28	28.90	28.82	28.93	O3LYP	29.24	28.78	28.80	28.82
OLYP	29.27	28.78	28.81	28.82	PBEh	28.99	28.61	28.55	28.66
PBE	29.21	28.82	28.76	28.86					
MGGA					**HM**				
mPWKCIS	29.29	28.89	28.83	28.90	MPW1KCIS	29.20	28.80	28.75	28.84
PBEKCIS	29.28	28.88	28.83	28.89	MPWKCIS1K	28.96	28.57	28.53	28.62
TPSSKCIS	29.13	28.75	28.69	28.79	PBE1KCIS	29.10	28.71	28.67	28.75
TPSS	29.03	28.66	28.60	28.72	TPSS1KCIS	29.04	28.66	28.60	28.71
VSXC	28.80	28.31	28.31	28.34	TPSSh	28.96	28.59	28.54	28.65

[a] Experiment: 28.47 eV; 28.01 eV (ref 109). Ab initio calculation (this study): 27.79 and 27.81 eV (MP2/TZQ and CCSDT/TZQ, respectively). All theoretical data were corrected with the value of 0.13 eV to account for the spin-orbit splitting in ^5D Ru^{2+}.

TABLE 4: Free Energy ΔG_I^o (in eV) of Gas-Phase Ionization of $[Ru(H_2O)_6]^{2+}$ [a]

Method	LANL2DZ	DZQ	MWB28	TZQ	Method	LANL2DZ	DZQ	MWB28	TZQ
GGA					**H**				
BLYP	15.79	15.73	15.55	15.70	B3LYP	16.28	16.18	15.94	16.07
BP86	15.89	15.82	15.64	15.79	B3P86	16.76	16.62	16.43	16.56
BPBE	15.80	15.71	15.53	15.66	B3PW91	16.21	16.07	15.84	16.01
BPW91	15.82	15.75	15.56	15.70	B97-1	16.18	16.08	15.88	15.99
G96LYP	15.74	15.67	15.48	15.64	B97-2	16.28	16.19	15.96	16.07
HCTH	16.19	16.06	15.86	15.99	B98	16.20	16.14	15.86	15.98
mPWLYP	15.83	15.77	15.58	15.73	BH&HLYP	16.61	16.53	16.25	16.35
mPWPBE	15.81	15.75	15.57	15.70	mPW1PW	16.18	16.12	15.87	15.97
mPWPW	15.82	15.78	15.60	15.74	O3LYP	16.14	16.05	15.83	15.94
OLYP	15.90	15.79	15.60	15.64	PBEh	16.18	16.06	15.82	15.94
PBE	15.81	15.72	15.53	15.66	*Average*	**16.30**	**16.20**	**15.97**	**16.09**
Average	**15.85**	**15.78**	**15.59**	**15.72**	*SD* [b]	**0.21**	**0.20**	**0.21**	**0.20**
SD [b]	**0.12**	**0.10**	**0.10**	**0.10**					
MGGA					**HM**				
BB95	15.79	15.73	15.56	15.70	B1B95	16.29	16.17	15.95	16.00
mPWB95	15.82	15.78	15.61	15.73	BB1K	16.46	16.38	16.12	16.20
mPWKCIS	15.88	15.78	15.60	15.73	MPW1B95	16.35	16.23	15.96	16.08
PBEKCIS	15.84	15.75	15.57	15.70	MPW1KCIS	16.13	16.04	15.83	15.94
TPSSKCIS	15.77	15.72	15.53	15.65	MPWKCIS1K	16.47	16.39	16.13	16.21
TPSS	15.74	15.70	15.51	15.62	PBE1KCIS	16.21	16.12	15.90	16.00
VSXC	16.50	16.42	16.21	16.33	MPWB1K	16.50	16.42	16.16	16.24
Average	**15.91**	**15.84**	**15.66**	**15.78**	TPSS1KCIS	16.02	15.89	15.67	15.82
SD [b]	**0.27**	**0.26**	**0.25**	**0.25**	TPSSh	15.94	15.81	15.62	15.74
					Average	**16.26**	**16.16**	**15.93**	**16.03**
					SD [b]	**0.20**	**0.22**	**0.20**	**0.18**

[a] Results of the TZQS calculations are omitted; they are identical to ΔG_I^o (TZQ) within 0.05 eV.

[b] Standard deviation

TABLE 5: Free Energy ΔG_I^o (in eV) of Gas-Phase Ionization of $[Ru(H_2O)_{18}]^{2+}$ [a]

Method	LANL2DZ	DZQ	MWB28	TZQ	Method	LANL2DZ	DZQ	MWB28	TZQ[b]
GGA					**H**				
BLYP	11.20	11.14	10.97	11.15	B3LYP	11.66	11.62	11.39	11.58
BP86	11.19	11.15	10.97	11.14	B3P86	12.02	11.98	11.76	11.92
BPBE	11.08	11.03	10.85	10.99	B3PW91	11.49	11.45	11.23	11.40
BPW91	11.12	11.07	10.89	11.03	B97-1	11.63	11.59	11.35	11.48
G96LYP	11.08	11.01	10.83	11.00	B97-2	11.55	11.50	11.28	11.47
HCTH	11.23	11.16	11.00	11.13	B98	11.63	11.60	11.35	11.50
mPWLYP	11.24	11.18	11.00	11.19	BH&HLYP	11.98	11.93	11.65	11.75
mPWPBE	11.11	11.06	10.89	11.04	mPW1PW	11.54	11.50	11.27	11.41
mPWPW	11.16	11.10	10.93	11.09	O3LYP	10.95	10.90	10.69	11.26
OLYP	10.84	10.68	10.55	10.62	PBEh	11.49	11.45	11.23	11.36
PBE	11.11	11.07	10.90	11.06	*Average*	**11.59**	**11.55**	**11.32**	**11.51**
Average	**11.12**	**11.06**	**10.89**	**11.04**	*SD* [c]	**0.29**	**0.30**	**0.28**	**0.19**
SD [c]	**0.11**	**0.14**	**0.13**	**0.15**					
MGGA					**HM**				
BB95	11.17	11.20	10.94	10.97	B1B95	11.60	11.44	11.26	11.48
mPWB95	11.25	11.32	11.06	11.15	BB1K	11.48	11.41	11.24	11.61
mPWKCIS	11.18	11.12	10.95	11.10	MPW1B95	11.40	11.33	11.16	11.53
PBEKCIS	11.19	11.13	10.96	11.12	MPW1KCIS	11.42	11.38	11.17	11.36
TPSSKCIS	11.13	11.08	10.89	11.02	MPWKCIS1K	11.81	11.77	11.51	11.63
TPSS	11.09	11.04	10.86	10.99	PBE1KCIS	11.54	11.50	11.27	11.43
VSXC	12.78	12.60	12.57	12.64	MPWB1K	11.43	11.38	11.18	11.66
Average	**11.40**	**11.36**	**11.18**	**11.28**	TPSS1KCIS	11.33	11.30	11.08	11.25
SD [c]	**0.61**	**0.56**	**0.62**	**0.60**	TPSSh	11.24	11.21	11.00	11.16
					Average	**11.47**	**11.41**	**11.21**	**11.46**
					SD [c]	**0.17**	**0.16**	**0.14**	**0.17**

[a] Geometry optimization and harmonic analysis for the $[Ru(H_2O)_{18}]^{3+}$ cluster at the TZQS level were performed using only GGA and MGGA type functionals. Results of the TZQS calculations are omitted; they are identical to ΔG_I^o (TZQ) within 0.05 eV.

[b] Zero-point energies for H/TZQ and HM/TZQ were taken from B3LYP/MWB28. [c] Standard deviation

TABLE 6: Partial Atomic Charges on the Metal and on the First and Second Hydration Shells in the $[Ru(H_2O)_n]^{q+}$ Clusters at the MPWB1K/LANL2DZ/6-31+G(d,p) Level

q	*n*	Ru Atom	1st Shell	2nd Shell
2+	6	0.61	1.39	
	18	0.48	0.97	0.55
3+	6	1.13	1.87	
	18	0.94	1.20	0.86

TABLE 7: Ionization Potentials I_e (in eV) Calculated by Wave Function Theory Methods [a]

Method	^{1}S Ru^{2+}	$[Ru(H_2O)_6]^{2+}$	$[Ru(H_2O)_{18}]^{2+}$
HF/TZQ	28.86	15.69	11.31
MP2/TZQ	29.91	16.28	11.52

[a] Values of I_e were calculated as the total energy difference at the equilibrium geometries of $[Ru(H_2O)_n]^{q+}$ (n = 6, 18; q = 2, 3) optimized at MPWB1K/MWB28.

TABLE 8: Free Energies of Solvation $\Delta\Delta G_S^o$ (in eV) with the First Hydration Shell Explicitly Included [a]

Method	LANL2DZ	DZQ	MWB28	TZQ	Method	LANL2DZ	DZQ	MWB28	TZQ
GGA					**H**				
BLYP	–10.69	–10.58	–10.56	–10.59	B3LYP	–10.84	–10.68	–10.66	–10.69
BP86	–10.72	–10.61	–10.61	–10.63	B3P86	–10.87	–10.72	–10.70	–10.76
BPBE	–10.73	–10.62	–10.61	–10.63	B3PW91	–10.86	–10.70	–10.69	–10.75
BPW91	–10.73	–10.62	–10.61	–10.63	B97-1	–10.81	–10.69	–10.67	–10.70
G96LYP	–10.69	–10.59	–10.58	–10.60	B97-2	–10.88	–10.76	–10.74	–10.78
HCTH	–10.78	–10.66	–10.65	–10.68	B98	–10.81	–10.70	–10.67	–10.71
mPWLYP	–10.69	–10.59	–10.57	–10.59	BH&HLYP	–10.99	–10.86	–10.82	–10.87
mPWPBE	–10.74	–10.63	–10.62	–10.64	mPW1PW	–10.85	–10.74	–10.71	–10.75
mPWPW	–10.73	–10.63	–10.61	–10.64	O3LYP	–10.82	–10.71	–10.69	–10.72
OLYP	–10.76	–10.63	–10.62	–10.65	PBEh	–10.89	–10.73	–10.72	–10.75
PBE	–10.74	–10.63	–10.62	–10.64	*Average*	**–10.86**	**–10.73**	**–10.71**	**–10.75**
Average	**–10.73**	**–10.62**	**–10.61**	**–10.63**	*SD* [b]	**0.05**	**0.05**	**0.05**	**0.05**
SD [b]	**0.03**	**0.02**	**0.03**	**0.03**					
MGGA					**HM**				
BB95	–10.71	–10.61	–10.61	–10.63	B1B95	–10.90	–10.74	–10.73	–10.76
mPWB95	–10.72	–10.62	–10.62	–10.64	BB1K	–10.95	–10.82	–10.80	–10.84
mPWKCIS	–10.71	–10.60	–10.59	–10.62	MPW1B95	–10.92	–10.76	–10.74	–10.78
PBEKCIS	–10.71	–10.60	–10.59	–10.62	MPW1KCIS	–10.82	–10.70	–10.68	–10.71
TPSSKCIS	–10.75	–10.64	–10.63	–10.65	MPWKCIS1K	–10.95	–10.82	–10.79	–10.83
TPSS	–10.76	–10.65	–10.64	–10.67	PBE1KCIS	–10.86	–10.74	–10.71	–10.75
VSXC	–10.89	–10.78	–10.78	–10.79	MPWB1K	–10.96	–10.84	–10.81	–10.85
Average	**–10.75**	**–10.64**	**–10.64**	**–10.66**	TPSS1KCIS	–10.83	–10.68	–10.67	–10.71
SD [b]	**0.06**	**0.06**	**0.06**	**0.06**	TPSSh	–10.82	–10.68	–10.67	–10.70
					Average	**–10.89**	**–10.75**	**–10.73**	**–10.77**
					SD [b]	**0.06**	**0.06**	**0.06**	**0.06**

[a] Solvation energies for the TZQS and TZQ gas-phase geometries are calculated at MWB28/6-31+G(d,p). Results of the TZQS calculations are omitted; they are identical to $\Delta\Delta G_S^o$ (TZQ) within 0.03 eV.

[b] Standard deviation

TABLE 9: Free Energies of Solvation $\Delta\Delta G_S^o$ (in eV) with the First and Second Hydration Shells Explicitly Included [a]

Method	LANL2DZ	DZQ	MWB28	TZQ	Method	LANL2DZ	DZQ	MWB28	TZQ
GGA					**H**				
BLYP	–7.14	–7.10	–7.00	–6.99	B3LYP	–7.26	–7.22	–7.11	–7.10
BP86	–7.21	–7.17	–7.07	–7.06	B3P86	–7.32	–7.28	–7.17	–7.17
BPBE	–7.19	–7.16	–7.06	–7.04	B3PW91	–7.29	–7.24	–7.14	–7.13
BPW91	–7.19	–7.16	–7.06	–7.04	B97-1	–7.27	–7.22	–7.12	–7.11
G96LYP	–7.15	–7.12	–7.02	–7.00	B97-2	–7.26	–7.22	–7.12	–7.09
HCTH	–7.06	–7.03	–6.95	–6.91	B98	–7.27	–7.23	–7.12	–7.11
mPWLYP	–7.15	–7.12	–7.01	–7.01	BH&HLYP	–7.38	–7.34	–7.22	–7.22
mPWPBE	–7.20	–7.17	–7.07	–7.06	mPW1PW	–7.30	–7.27	–7.17	–7.16
mPWPW	–7.20	–7.17	–7.07	–7.06	O3LYP	–7.02	–7.00	–6.91	–6.90
OLYP	–6.95	–6.93	–6.85	–6.83	PBEh	–7.31	–7.27	–7.17	–7.16
PBE	–7.20	–7.17	–7.06	–7.06	*Average*	**–7.27**	**–7.23**	**–7.13**	**–7.12**
Average	**–7.15**	**–7.12**	**–7.02**	**–7.01**	*SD* [b]	**0.09**	**0.09**	**0.08**	**0.08**
SD [b]	**0.08**	**0.07**	**0.07**	**0.07**					
MGGA					**HM**				
BB95	–7.15	–7.11	–7.02	–6.99	B1B95	–7.27	–7.24	–7.13	–7.12
mPWB95	–7.16	–7.13	–7.03	–7.01	BB1K	–7.34	–7.29	–7.18	–7.14
mPWKCIS	–7.17	–7.13	–7.03	–7.02	MPW1B95	–7.31	–7.27	–7.16	–7.11
PBEKCIS	–7.17	–7.13	–7.03	–7.02	MPW1KCIS	–7.23	–7.19	–7.11	–7.08
TPSSKCIS	–7.20	–7.17	–7.07	–7.05	MPWKCIS1K	–7.35	–7.30	–7.20	–7.18
TPSS	–7.22	–7.19	–7.09	–7.08	PBE1KCIS	–7.27	–7.23	–7.12	–7.11
VSXC	–7.45	–7.44	–7.38	–7.35	MPWB1K	–7.36	–7.32	–7.21	–7.15
Average	**–7.22**	**–7.18**	**–7.09**	**–7.07**	TPSS1KCIS	–7.26	–7.22	–7.12	–7.10
SD [b]	**0.10**	**0.11**	**0.13**	**0.12**	TPSSh	–7.26	–7.23	–7.13	–7.11
					Average	**–7.30**	**–7.25**	**–7.15**	**–7.12**
					SD [b]	**0.05**	**0.04**	**0.04**	**0.03**

[a,b] See footnotes to Table 8

TABLE 10: Components of ΔG_S^0 (in eV) at the MPWB1K/MWB28 Level as Functions of the Ru atomic radius (in Å)

ρ_{Ru}	q	n	$\Delta G°_S$	ΔG_{EP}	G_{CDS}
2.00	2+	6	–8.81	–8.61	–0.20
		18	–6.90	–6.12	–0.78
2.00	3+	6	–19.67	–19.50	–0.16
		18	–14.05	–13.32	–0.73
1.74	2+	6	–8.82	–8.62	–0.20
		18	–6.93	–6.15	–0.78
1.74	3+	6	–19.69	–19.52	–0.16
		18	–14.06	–13.33	–0.73
2.26	2+	6	–8.79	–8.58	–0.20
		18	–6.85	–6.07	–0.78
2.26	3+	6	–19.62	–19.46	–0.16
		18	–14.05	–13.32	–0.73

TABLE 11: Standard Reduction Potential $E^{o}_{Ru^{3+}|Ru^{2+}}$ (in V) with the First Hydration Shell Explicitly Included [a]

Method	LANL2DZ	DZQ	MWB28	TZQ	Method	LANL2DZ	DZQ	MWB28	TZQ
GGA					**H**				
BLYP	0.81	0.86	0.70	0.83	B3LYP	1.17	1.22	1.00	1.10
BP86	0.89	0.93	0.75	0.88	B3P86	1.61	1.63	1.45	1.52
BPBE	0.79	0.82	0.64	0.75	B3PW91	1.07	1.09	0.87	0.98
BPW91	0.82	0.85	0.67	0.79	B97-1	1.09	1.11	0.93	1.01
G96LYP	0.77	0.80	0.62	0.76	B97-2	1.12	1.15	0.94	1.02
HCTH	1.12	1.12	0.93	1.03	B98	1.11	1.16	0.91	1.00
mPWLYP	0.86	0.90	0.73	0.86	BH&HLYP	1.34	1.39	1.14	1.20
mPWPBE	0.79	0.84	0.67	0.78	mPW1PW	1.04	1.10	0.88	0.95
mPWPW	0.81	0.88	0.70	0.82	O3LYP	1.03	1.06	0.86	0.94
OLYP	0.87	0.87	0.70	0.72	PBEh	1.01	1.05	0.82	0.91
PBE	0.79	0.81	0.63	0.74	*Average*	**1.16**	**1.19**	**0.98**	**1.06**
Average	**0.85**	**0.88**	**0.71**	**0.81**	*SD* [b]	**0.18**	**0.18**	**0.19**	**0.18**
SD [b]	**0.10**	**0.09**	**0.09**	**0.09**					
MGGA					**HM**				
BB95	0.79	0.84	0.67	0.80	B1B95	1.11	1.15	0.95	0.96
mPWB95	0.82	0.87	0.71	0.81	BB1K	1.23	1.27	1.04	1.08
mPWKCIS	0.89	0.90	0.73	0.83	MPW1B95	1.15	1.18	0.94	1.02
PBEKCIS	0.85	0.87	0.69	0.80	MPW1KCIS	1.03	1.06	0.87	0.95
TPSSKCIS	0.75	0.80	0.62	0.72	MPWKCIS1K	1.24	1.29	1.06	1.09
TPSS	0.70	0.77	0.59	0.67	PBE1KCIS	1.07	1.11	0.90	0.97
VSXC	1.33	1.35	1.16	1.26	MPWB1K	1.25	1.30	1.07	1.10
Average	**0.87**	**0.92**	**0.74**	**0.84**	TPSS1KCIS	0.91	0.93	0.72	0.82
SD [b]	**0.21**	**0.20**	**0.19**	**0.19**	TPSSh	0.84	0.85	0.67	0.75
					Average	**1.09**	**1.13**	**0.91**	**0.97**
					SD [b]	**0.15**	**0.16**	**0.14**	**0.12**

[a] Results of the TZQS calculations are omitted; they are identical to $E^{o}_{Ru^{3+}|Ru^{2+}}$ (TZQ) within 0.05 V.

[b] Standard deviation

TABLE 12: Standard Reduction Potential $E^{o}_{Ru^{3+}|Ru^{2+}}$ (in V) with the First and Second Hydration Shells Explicitly Included [a]

Method	LANL2DZ	DZQ	MWB28	TZQ	Method	LANL2DZ	DZQ	MWB28	TZQ
GGA					**H**				
BLYP	–0.22	–0.24	–0.31	–0.12	B3LYP	0.13	0.12	0.00	0.20
BP86	–0.29	–0.30	–0.37	–0.20	B3P86	0.42	0.42	0.31	0.47
BPBE	–0.39	–0.41	–0.49	–0.34	B3PW91	–0.07	–0.07	–0.19	–0.01
BPW91	–0.35	–0.37	–0.45	–0.29	B97-1	0.08	0.09	–0.05	0.09
G96LYP	–0.36	–0.38	–0.47	–0.28	B97-2	0.01	0.01	–0.12	0.10
HCTH	–0.11	–0.15	–0.23	–0.06	B98	0.08	0.09	–0.05	0.11
mPWLYP	–0.20	–0.22	–0.29	–0.09	BH&HLYP	0.31	0.31	0.15	0.25
mPWPBE	–0.37	–0.39	–0.46	–0.30	mPW1PW	–0.05	–0.05	–0.18	–0.03
mPWPW	–0.33	–0.35	–0.42	–0.25	O3LYP	–0.35	–0.37	–0.50	0.08
OLYP	–0.39	–0.53	–0.58	–0.49	PBEh	–0.09	–0.10	–0.22	–0.08
PBE	–0.37	–0.38	–0.45	–0.28	*Average*	**0.05**	**0.05**	**–0.08**	**0.12**
Average	**–0.31**	**–0.34**	**–0.41**	**–0.25**	*SD* [b]	**0.22**	**0.22**	**0.22**	**0.16**
SD [b]	**0.09**	**0.10**	**0.10**	**0.12**					
MGGA					**HM**				
BB95	–0.27	–0.20	–0.36	–0.29	B1B95	0.04	–0.08	–0.14	0.08
mPWB95	–0.19	–0.09	–0.26	–0.14	BB1K	–0.14	–0.16	–0.23	0.19
mPWKCIS	–0.27	–0.29	–0.36	–0.20	MPW1B95	–0.19	–0.22	–0.27	0.14
PBEKCIS	–0.26	–0.27	–0.35	–0.18	MPW1KCIS	–0.09	–0.09	–0.22	0.00
TPSSKCIS	–0.36	–0.37	–0.46	–0.31	MPWKCIS1K	0.18	0.18	0.03	0.17
TPSS	–0.41	–0.42	–0.51	–0.36	PBE1KCIS	–0.01	–0.01	–0.13	0.04
VSXC	1.05	0.89	0.91	1.02	MPWB1K	–0.22	–0.21	–0.31	0.23
Average	**–0.10**	**–0.11**	**–0.20**	**–0.07**	TPSS1KCIS	–0.21	–0.21	–0.32	–0.13
SD [b]	–0.27	–0.20	–0.36	–0.29	TPSSh	–0.30	–0.30	–0.41	–0.23
					Average	**–0.10**	**–0.12**	**–0.22**	**0.05**
					SD [b]	**0.15**	**0.14**	**0.13**	**0.15**

[a, b] See footnotes to Table 11

TABLE 13: Free Energies of Solvation $\Delta\Delta G_S^o$ (in eV): SM6 versus IEF-PCM [a]

Method	*n*	SM6	IEF-PCM/UFF	IEF-PCM/UAHF	IEF-PCM/Bondi
BLYP/MWB28	6	–10.56	–10.24	–11.39	–10.28
BLYP/MWB28	18	–7.00	–6.61	–6.59	–6.65
B3LYP/LANL2DZ	6	–10.84	–10.33	–11.42	–10.39
B3LYP/LANL2DZ	18	–7.26	–6.64	–6.62	–6.68
MPWB1K/DZQ	6	–10.84	–10.39	–11.40	–10.46
MPWB1K/DZQ	18	–7.32	–6.62	–6.63	–6.74

[a] Gas-phase geometries were optimized at the corresponding level of theory. We used the following models for atomic radii in the IEF-PCM calculations: the united-atom universal force field topological model (UFF), the united-atom Hartree-Fock model (UAHF), and the Bondi atomic radii (Bondi).

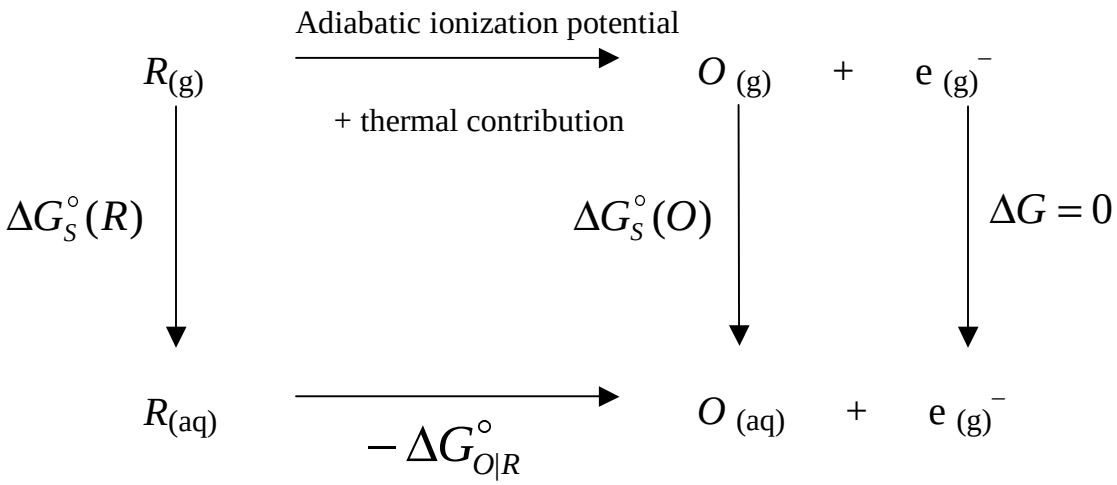
Adiabatic ionization potential
$R_{(g)}$
$O_{(g)}$ + $e_{(g)}^-$
+ thermal contribution
$\Delta G_S^\circ(R)$
$\Delta G_S^\circ(O)$
$\Delta G = 0$
$R_{(aq)}$
$O_{(aq)}$ + $e_{(g)}^-$
$-\Delta G_{O|R}^\circ$

Scheme 1

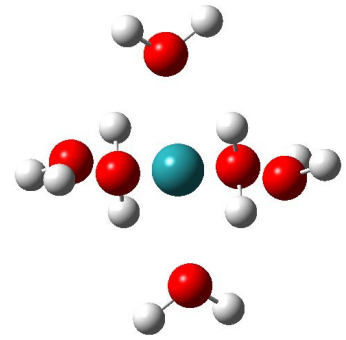

(a) C_i

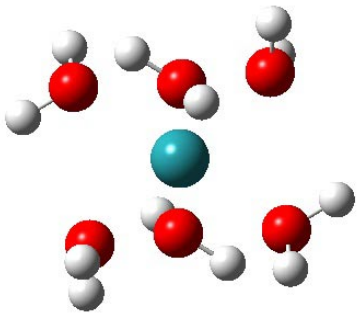

(b) S_6

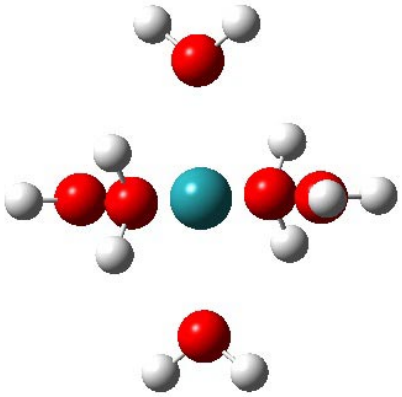

(c) T_h

Figure 1. Conformations of the $[Ru(H_2O)_6]^{2+/3+}$ Clusters.

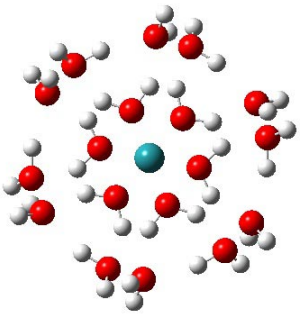

(a) ***S*$_6$**, Top View

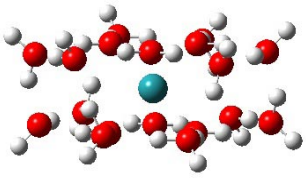

***S*$_6$**, Side View

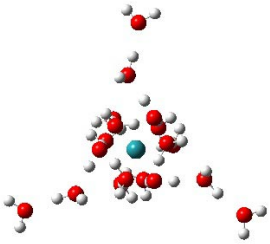

(b) ***C*$_3$ (6,9,3)**, Top View

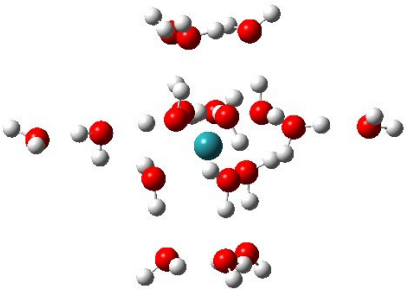

***C*$_3$ (6,9,3)**, Side View

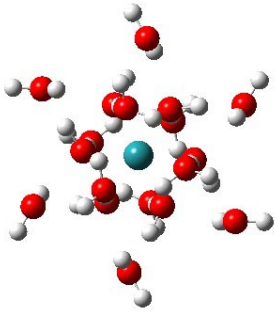

(c) ***C*$_3$ (6,12)**, Top View

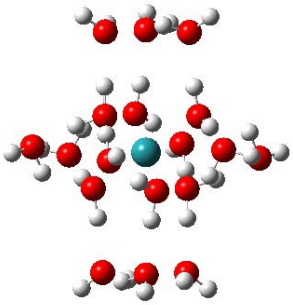

***C*$_3$ (6,12)**, Side View

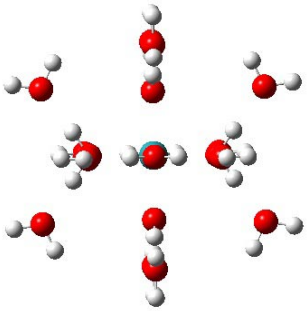

(d) ***T*$_h$**, Top View

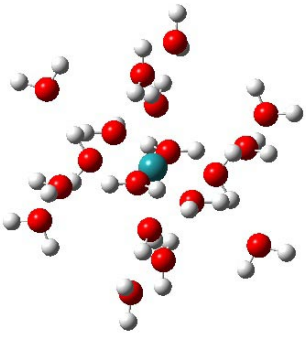

***T*$_h$**, Side View

Figure 2. Conformations of the $[Ru(H_2O)_{18}]^{2+/3+}$ Clusters.